University of Alberta
Printing Department

THE UNIVERSITY OF ALBERTA

THE DECOMPOSITION KINETICS OF ZINC-ALUMINUM ALLOYS

A THESIS

SUBMITTED TO THE FACULTY OF GRADUATE STUDIES

IN PARTIAL FULFILMENT OF THE REQUIREMENTS FOR THE DEGREE

OF MASTER OF SCIENCE

DEPARTMENT OF MINING AND METALLURGY

by

DONALD RAE GREKUL

EDMONTON, ALBERTA

APRIL, 1960

UNIVERSITY OF ALBERTA

FACULTY OF GRADUATE STUDIES

The undersigned certify that they have read, and recommend to the Faculty of Graduate Studies for acceptance, a thesis entitled

THE DECOMPOSITION KINETICS
OF ZINC-ALUMINUM ALLOYS

submitted by DONALD RAE GREKUL

in partial fulfilment of the requirements for the degree of Master of Science.

ABSTRACT:

A rate equation is developed from absolute reaction rate theory to enable a direct treatment of experimental data in the study of the decomposition rates of a metastable phase in alloys. The various parameters affecting decomposition are explicitly defined and their effect on the activation energy is elaborated.

The rate of decomposition of the quenched α-phase (in metastability) is studied in zinc-aluminum alloys containing forty, forty-five and fifty-five weight percent aluminum. The relative intensity ratios of X-ray reflections from particular α-phase and β-phase planes were related to alloy composition and used to measure the decomposition rates of the supersaturated α-phase at different temperatures. The technique necessitated an extensive literature survey to substantiate the validity of the zinc-aluminum constitutional diagram.

The activation energy associated with the decomposition of α increases with aluminum content, and varies between 18.6 and 25.0 kcal./mole for the alloys studied. A diffusion model has been proposed that involves the advance of β-phase interfaces into the α-phase to produce long, rod-like precipitates. The self-diffusion of zinc in the α-matrix is believed to be the rate controlling mechanism.

ACKNOWLEDGEMENTS:

The author wishes to express his gratitude to Dr. J.G. Parr, who capably supervised this thesis, and to Dr. W.V. Youdelis for his welcomed assistance and criticism in the development of the relevant theory. He also appreciates the assistance of Mr. R. M. Scott in the preparation of metallographic samples.

The author is particularly grateful to The Consolidated Mining and Smelting Company of Canada Limited, whose financial aid made this work possible, and to the staff of the company's Research and Development Division for their friendly encouragement.

TABLE OF CONTENTS

ILLUSTRATIONS:

ILLUSTRATIONS (continued):

TABLES (APPENDIX II):

INTRODUCTION

A determination of the decomposition kinetics of a metastable phase in an alloy system involves the measurement of breakdown speeds at different temperatures. The study described in this thesis was conducted on three alloys of aluminum and zinc (namely forty, forty-five, and fifty-five weight percent aluminum*) which were quenched to retain the supersaturated face-centered cubic α-phase (in metastability), and then tempered at temperatures between 75° C. and 150° C. to produce equilibrium structures of α and β (close-packed hexagonal). See Figure 1.[1]

While many eutectoid systems show a sluggish eutectoidal transformation, the zinc-aluminum eutectoid reaction is rapid. This phenomenon presents problems in the study of decomposition since the high temperature single phase is difficult to retain in alloys containing less than thirty-three percent aluminum. For this reason the studies have been limited to alloys of higher aluminum content.

The technique for measuring decomposition rates required that the zinc-aluminum diagram be firmly established. An extensive literature survey was conducted on the equilibrium diagram and is presented in the following section.

---

* weight percents are used throughout unless otherwise stated.

Many investigations into decomposition rates have been carried out by previous workers, who have developed equations for precipitation rates that are modifications of the general nucleation and growth equations.[2, 3] The assumption is usually made that the decomposition rate follows the rate law as given by the equation[4]

$$\frac{dX}{dt} = K(1 - X)t^m \qquad \ldots (1)$$

where X is the fraction transformed, K is a rate constant and m is a constant whose value depends upon the precipitate shape. There does not seem to be a formal derivation of this equation for decomposition rates.

In the study of decomposition rates by Roberts, Averbach and Cohen,[2] by Polonis and Parr,[5] and by Owen,[4] equation 1 is used. The rate constant K is not the same as the rate constant of the Arrhenius equation and consequently does not give the true activation energy. The same investigators surmised that the following treatment should give the true activation energy:

Integrating equation 1 and taking natural logarithms:

$$\ln \ln\left(\frac{1}{1 - X}\right) = \ln\left(\frac{K}{m + 1}\right) + (m + 1) \ln t \ldots (2)$$

Consequently a plot of $\ln \ln\left(\frac{1}{1 - X}\right)$ versus $\ln t$ gives a straight line of slope $(m + 1)$ and intercept $\ln\left(\frac{K}{m + 1}\right)$ on the ordinate. Since it is assumed that $K = K_o e^{-Qk/RT}$, a plot of ordinate intercept (i. e. $\ln\left(\frac{K}{m + 1}\right)$) versus $1/T$ gives a straight line of slope $-Qk/R$. Because K is expressed in units time $^{-(m + 1)}$ while the units of the rate

constant in the Arrhenius equation are in time^{-1}, it is argued that the true activation energy (Qt) is $\frac{Qk}{m+1}$.

The general equation has specific applications to recrystallization where the growth rates are constant (to a good approximation) but it will not necessarily apply to decomposition mechanisms where growth rates are affected by concentration gradients. Although the described treatment has given satisfactory results in some cases (as surmised from the magnitude of activation energies obtained) it appears to have given anomalous results in other systems.

The treatment is, therefore, in some doubt and an alternative method is proposed. In this thesis an expression for decomposition rate is derived which is similar to equation 1 but in which the various parameters are explicitly defined to enable a more direct treatment of the experimental data.

LITERATURE SURVEY OF THE ZINC-ALUMINUM PHASE DIAGRAM

The equilibrium diagram of the zinc-aluminum system has been a topic of contention since the beginning of this century. Most controversy has arisen over the possible existence of a peritectic reaction at 440° C. Recently, however, with the advent of high temperature X-ray diffraction techniques, the phase diagram shown in Figure 1 has been firmly established.

As early as 1911, the zinc-rich end of the diagram was determined with reasonable accuracy. Rosenhain and Archbutt[6] showed by thermal analysis that in addition to a eutectic arrest a peritectic reaction appeared to occur at 443° C., at which temperature, they suggested, the aluminum-rich solid solution reacted with liquid to form a constituent Al_2Zn_3. Although the peritectic appeared to be verified by thermal data its presence could not be affirmed by microscopic examination.

Bauer and Vogel's[7] investigations of the peritectic reaction at 443° C. placed the limits of the peritectic horizontal at 60 percent and 78 percent zinc. They found that the eutectoid horizontal reaction at 256° C. extended to 25 percent zinc at the aluminum-rich end. Between 256° C. and 443° C. a two-phase region was thought to exist. However, a two phase alloy could not be retained by quenching appropriate compositions from 443° C.

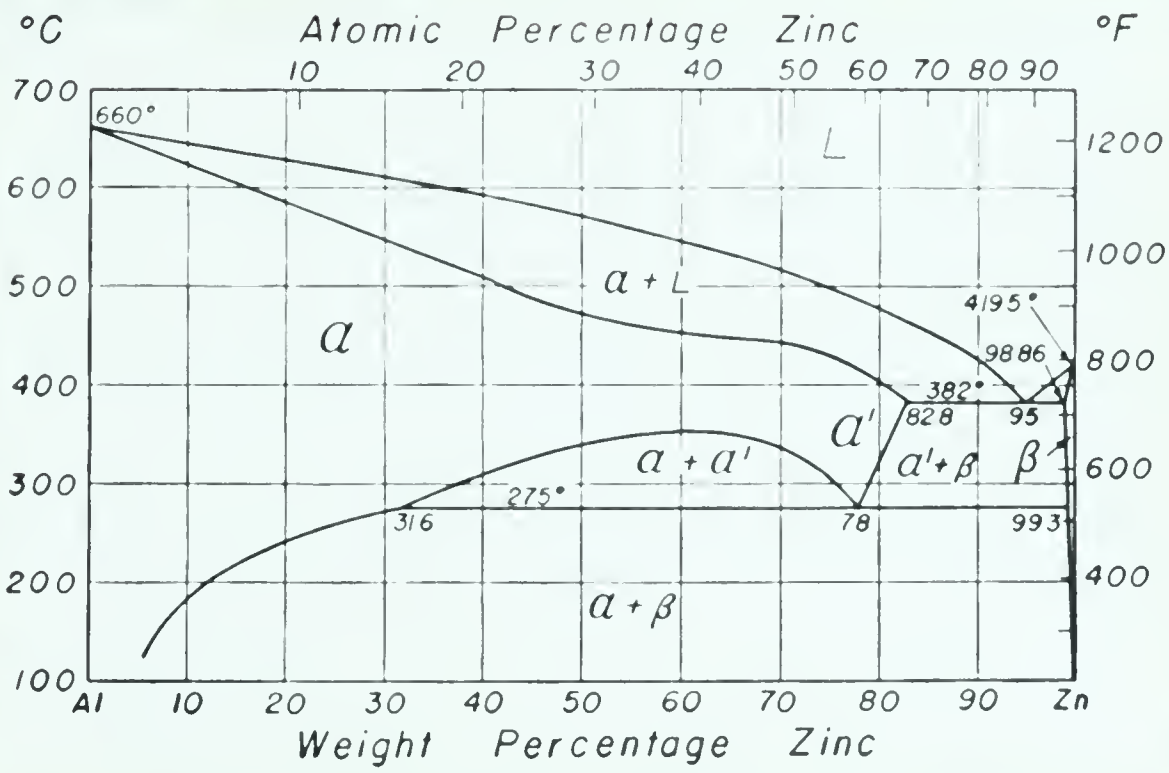

Figure 1. Zinc-Aluminum Constitutional Diagram

D. Hanson and M. L. V. Gayler[8] investigated the peritectic reaction by quenching alloys (40 percent to 80 percent zinc) from temperatures within the proposed two-phase field. The shape of the two phase region was determined from these experiments. The shape of the solidus was predicted from microscopic examination of alloys which were heated to their respective melting points and then quenched. The eutectic reaction found at 380° C. extended to 82 percent zinc. Contrary to the results of Bauer and Vogel, the transformation at 256° C. ended at 35 percent zinc. Because the microstructures of the reaction at 256° C. were typical of eutectoid transformations, the possibility of an Al_2Zn_3 compound was rejected, although the peritectic reaction was still presumed to be present.

T. Tanabe[9] used resistivity-temperature measurements to investigate the equilibrium diagram. Tanabe measured the change in resistance that occurs when an alloy is heated from room temperature to the liquid region. The liquidus, solidus, peritectic and solid solubility lines agreed with the results of Hanson and Gayler. A narrow peritectic horizontal was thought to lie between 70 percent and 69 percent zinc. Tanabe used thermal analyses and thermal expansion techniques to place the eutectoid reaction at 270° C. The solid solubility of aluminum zinc was found to be 1.0 at 385° C., 0.5 percent at 270° C., and 0.9 percent at room temperature.

T. Isihara[10] employed the methods of resistivity, dilatometry, microscopy and X-ray diffraction for investigation of the diagram. The room temperature solubility of zinc in aluminum was 23 percent, while the solubility of aluminum in zinc was 0.3 percent. The eutectoid at 280° C. and 79 percent zinc produced two solid solutions containing 99.7 percent and 35 percent zinc. The eutectic at 380° C. and 95 percent zinc was associated with a eutectic horizontal between 99 percent and 83 percent zinc. Isahara suggested that the β-phase was a "solid solution with an unknown concealed compound" similar to that suggested by Rosenhain and Archbutt. The peritectic horizontal at 440° C. occurred between 59 percent and 87 percent zinc..

The resistivity-temperature measurements by W. L. Fink and L.A. Wiley[11] verified previous determinations of the solubility of zinc in aluminum between 125° C. and 275° C. A distinct break in solid solubility was noted at 275° C. where the solubility of zinc in aluminum increased from 31.6 percent to 77.7 percent. The solubility increased slowly between 275° C. and 350° C. Microscopy showed that two phases were present if an alloy was quenched from 335° C., but a single, homogeneous phase was retained if the alloy was quenched from 365° C. For the region above 275° C., Fink and Wiley proposed a solubility gap where two phases were in equilibrium and had the same composition at 353° C. Although other investigators[12] found

two phases above this gap, the X-ray work by Fink and Wiley depicted a single phase field. The possibility of a loop on the solidus curve was not excluded. Fink and Wiley predicted that as impurities increased, both loops grew large until, possibly, they joined.

In 1938 M. L. V. Gayler and E. G. Sutherland[13] published a paper which primarily dealt with the nature of the thermal change at 443° C. Alloys (68, 68.5, 69 and 70.5 percent zinc) heat treated at 355° C. showed evidence of two phases, while the same alloys heat treated at 430° C. showed only one phase. The solidus was redetermined by the thermal analysis of alloys (60 percent to 84 percent zinc) heated and cooled between 440° C. and 450° C. Gayler and Sutherland predicted that no peritectic was present in the zinc aluminum diagram for the following reasons: (a) the liquidus showed no inflection, (b) no constant temperature reaction occurred on heating or cooling, (c) a marked change in solid solubility of zinc in aluminum occurred over a small range in temperature, which would account for the heat change observed and exclude the possibility of a new phase. That is, the heat change was attributed to the marked change in composition of the solid phase crystallizing from the liquid state.

High temperature X-ray diffraction techniques were used by Elwood[14, 15] for determining the validity of the zinc-aluminum phase diagram. Lattice parameter measurements were made of

alloys held at temperatures within the solid, and solid and liquid regions. In the $\alpha + \alpha'$ region, the lattice parameter of the two phases (both face-centered cubic) were dependent on temperature, but independent of alloy composition. At 360° C. the lattice parameters of the two phases became identical which suggested that the two phases became a single phase. In the homogeneous field above 360° C. each alloy had a characteristic parameter. Since no horizontal was present on a plot of lattice parameter versus atomic percent zinc, a single phase field was assumed to exist above 360° C. The lattice parameters measured in the liquid and solid region represented solid-liquid equilibrium and were dependent upon the solubility at a particular temperature. If a peritectic were present in the system, it would have appeared as a phase change along the solidus. There was no evidence of such a change. The results agreed with those of Gayler and Sutherland.

Judging from the multitude of data and the agreement between later investigators who used more exact techniques, it may be concluded that the present zinc-aluminum diagram is valid. A theoretical verification of the diagram is presented in the theory section of this thesis.

THEORY

a) Zinc-Aluminum Constitutional Diagram

The eutectic and eutectoid reactions in the constitutional diagram need no verification since they obey the phase rule and are common in alloy systems. Furthermore, the solid solubilities of zinc in aluminum and aluminum in zinc are well established.[11] However, the flattening of the solidus and existence of the solubility gap should be verified.

Consider an alloy (for example, 69 percent zinc) cooled slowly through the liquidus and solidus. When the liquidus is reached solid of some concentration separates from the liquid. This solid is stable at this temperature, but presumably has Brillouin-zones which are not filled.[8] Cooling further could cause electronic configurations to change with a subsequent filling of Brillouin-zones and production of lattice vacancies. These vacancies provide space for an increase in solubility of zinc which also facilitates the filling of Brillouin-zones for stability. It is possible, therefore, that a large number of vacancies are produced by a small drop in temperature. This would permit a marked increase in zinc solubility and would produce a large change in solid composition. This phenomenon, in itself, could cause the solidus to flatten and is supported by the work of Gayler and Sutherland[13] and Elwood[15].

The existence of the solubility gap ($\alpha + \alpha'$) can be

verified by making an analogy to the immiscibility field for two-phase equilibria of liquids. Inside the immiscibility gap, the composition of α exists in equilibrium with the conjugate composition of α'. Increasing the temperature decreases the composition difference between the phases α and α' until the two phases are identical[15] at the so-called critical point (360° C.)[16]. Above 365° C. only one phase should exist over the entire range of composition according to this analogy. Actually this is what happens, since α and α' have the same crystal structure, and differ only in lattice parameter (which changes with concentration).

b) Theory of Decomposition Kinetics

In the following a new rate expression is developed in which the parameters of decomposition are explicitly defined, enabling a more direct treatment of the experimental data than that of previous investigators[2, 3, 4, 5] who started with the general equation (1).

For simplicity the growth rates of a precipitate grain in all directions will be considered equal and the assumption made that the growth rate is controlled by the diffusion rate of the principal component in the matrix. . . The concentration of the principal component (C_β) is assumed constant in the precipitate and higher than its mean concentration (C_α) in the alloy. The rate of advance of an interface is then proportional to the flux of the principal com-

ponent in the direction opposite that of growth. Furthermore, local equilibrium is assumed at the interface. That is, the concentration (C_e) at interface remains constant. The validity of this assumption has been shown in alloy solidification[17, 18] where the advance of the solid-liquid interface during solidification provides a close analogy to the advance of a solid-solid interface.

A growth model representing the above conditions (for one interface) is shown in Figure 2.

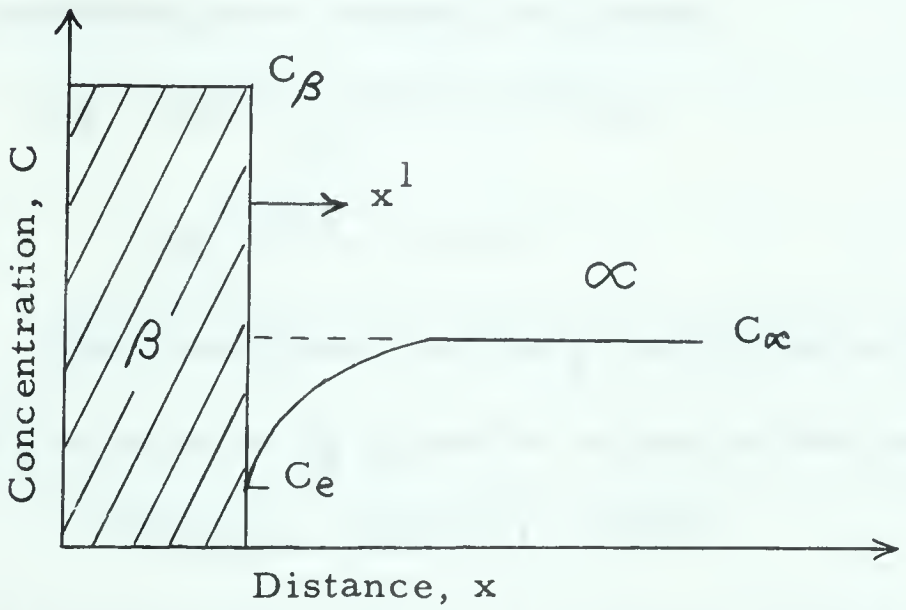

Figure 2. Advancing interface during the growth of β precipitate.

Zener[19] has solved the diffusion equation for the system represented in Figure 2. The expression he gives for the rate of advance of the precipitate in one dimension is

$$G_x = K_1 D^{1/2} t^{-1/2} \qquad \ldots (3)$$

where D is the diffusion coefficient (assumed independent of concentration) and t is the growth time. K_1 is related to the concentrations C_β, C_α and C_e in the dimensionless combination,

$$K_1 = K_2 \frac{(C\alpha - C_e)}{(C_\beta - C\alpha)^{1/2}(C_\beta - C_e)^{1/2}} \quad \ldots (4)$$

where K_2 varies from 1.13 to 1.41 as C_α varies from C_e to C_β.

The dimension of precipitate in the x-direction is given by

$$D_x = \int_o^{t-t^1} G_x dt \quad \ldots\ldots\ldots (5)$$

where t is the time from the start of the decomposition process and t^1 the time required for nucleation (more specifically the nucleation period for the grain in question). Substituting equation 3 in 5 and integrating with respect to t yields

$$D_x = K_1 D^{1/2} \int_o^{t-t^1} t^{-1/2}\, dt$$

$$= 2K_1 D^{1/2}(t - t^1)^{1/2} \quad \ldots\ldots\ldots (6)$$

The assumption that the growth rates in the other two directions are equal to G_x gives the volume of the precipitate grain as

$$v = fD_xD_yD_z = fKD^{3/2}(t - t^1)^{3/2} \quad \ldots\ldots\ldots (7)$$

where f is a shape factor and K is a constant which includes those appearing in the expressions for the dimensions.

If $\dot{N}$ is the nucleation frequency per unit volume, the number of grains, dn, originating in time, dt^1, where t^1 is the nucleation period, is

$$dn = \dot{N}(1 - X)dt^1 \quad \ldots\ldots\ldots (8)$$

where X represents the fraction of total decomposition.

There is present, however, impingement in the decomposition process in the sense that there is interaction of diffusion fields of the growing precipitate, and consequently a depletion of

the pertinent component. This is analogous to impingement of grains during recrystallization which has been treated rigorously by Avrami[20]. Using Avrami's treatment, a number of grains dn^1 is defined as

$$dn^1 = dn + \dot{N} X dt^1 = \dot{N} dt^1$$

where $\dot{N} X dt^1$ is the number of phantom grains that would have originated in volume v had it not decomposed. The fraction of volume transformed, disregarding impingement, is then

$$X_{ex} = \int_o^t v dn^1 = fKD^{3/2} \int_o^t (t - t^1)^{3/2} \dot{N} dt^1 \quad . \quad . \quad . \quad (11)$$

Avrami has shown that the relationship between X_{ex} and X is,

$$\frac{dX}{dX_{ex}} = 1 - X \quad . \quad . \quad . \quad (12)$$

Qualitatively, this expression may be arrived at in the following way: the average nucleation frequency throughout a unit volume is the same. The fraction decomposed in the unstable matrix is dX in time dt. The fraction that would have decomposed during the same time in the unit (total) volume is simply the ratio of the unit volume to the undecomposed volume times dX; i. e. $\left(\frac{1}{1 - X}\right) dX = dX_{ex}$, which is equivalent to equation 12.

Integration of equation 12 yields,

$$\int_o^{X_{ex}} dX_{ex} = X_{ex} = \int_o^X \left(\frac{1}{1 - X}\right) dX = -\ln(1 - X) \quad . \quad . \quad . \quad (13)$$

Combining equations 11 and 13,

$$-\ln (1 - X) = fKD^{3/2} \int_o^t (t - t^1)^{3/2} \dot{N} dt^1 \quad . \quad . \quad . \quad . \quad . \quad (14)$$

Now an expression must be found for the nucleation frequency $\dot{N}$. Nucleation in the solid state has been admirably treated by Avrami. He proposed that the new phase is nucleated by sub-microscopic "germ nuclei" which already exist in the old phase and whose effective number can be altered by temperature and duration of superheating. The germ nuclei may consist of heterogeneities of any type, most frequently foreign particles or chemical inhomogeneities.

The germ nuclei are depleted in two ways and their number $N = N(t^1)$ decreases from the original amount $\bar{N}$. First, some of them become active nuclei $\left[N' = N^1(t^1)\right]$ in consequence of free energy fluctuations that may arise from size, concentration or order fluctuations which enable them to jump across the boundary of the metastable region. The probability that this happens is given by γN where $\gamma = \gamma(T)$, the probability of formation of growth nucleus per germ nucleus per unit time. From absolute reaction rate theory it can be shown that

$$\gamma = \gamma_o \; e^{-Q_n/RT} \; e^{-\Delta F^*/RT} \quad . \; . \; . \; . \; (15)$$

where Q_n is the activation energy for the formation of the nuclei, ΔF^* is the free energy of formation of an embryo of critical size which becomes a growth nucleus, R is the universal gas constant and T is the absolute temperature. If the process of formation of growth nuclei is considered to be a bimolecular reaction between

the germ nuclei surrounded by their subscritical shells of the precipitating phase, then Q_n is the experimental activation energy (assuming that the separation of the experimental activation energy from the true activation energy has been made and included in γ_0) for the transfer of an atom across the precipitate interface into the precipitate. This activation energy is less than the activation energy for diffusion since a jump of this sort presumably involves less disturbance of the neighbouring atoms than would a normal diffusion jump. Furthermore, this activation energy is relatively independent of temperature.

The free energy of formation (ΔF^*) of the growth nucleus is a function of the interfacial free energy and volume free energy on the formation of the precipitate. Therefore $\Delta F^* = \Delta F(T)$, which indicates that γ is a function of the degree of supercool. If the sum of ΔF^* and Q_n is large, γ will be small and then the germ nuclei are depleted by being ingested by the growing grains. If the number thus ingested in time t^1 is $N^{11} = N^{11}(t^1)$ then

$$dN = -dN^1 - dN^{11}$$

$$dN^1 = \gamma N dt'$$

$$dN^{11} = \bar{N} dV \qquad \ldots . (16)$$

If γ is large, then dN^{11} is small in comparison to dN^1 so that

$$\frac{dN}{dt^1} = \frac{-dN^1}{dt^1} = -\gamma N \qquad \ldots . (17a)$$

Integration of equation 17 yields

$$N = \bar{N}\, e^{-\gamma t^1} \qquad \ldots\ (17b)$$

The nucleation rate per unit volume, $\dot{N}$, is given by

$$\dot{N} = \frac{dN}{dt^1} = \frac{-dN^1}{dt^1} = \bar{N}\,\gamma\, e^{-\gamma t^1} \qquad \ldots\ (18)$$

If γ is small and the germ nuclei are numerous, Avrami has shown that as $N \rightarrow \infty$, $\gamma \rightarrow 0$ and $\gamma N \rightarrow$ finite number; a finite rate of spontaneous nucleation is (to a good approximation) given by

$$\dot{N} = \gamma \bar{N} \qquad \ldots\ (19)$$

Using these two extreme conditions, the solution of equation 14 can now be given. For γ large,

$$\ln (1 - X) = -fKD^{3/2}\, \bar{N}\, \gamma \int_o^t (t - t^1)^{3/2}\, e^{-\gamma t^1}\, dt^1 \qquad \ldots\ (20)$$

Integrating equation 20 by parts, the equation approximates to,

$$-\ln (1 - X) = fKD^{3/2}\, \bar{N}\, t^{3/2}$$

or

$$X = 1 - e^{-fKD^{3/2} t^{3/2} \bar{N}} \qquad \ldots\ (21)$$

For γ very small,

$$\ln (1 - X) = -fKD^{3/2}\, \bar{N}\, \gamma \int_o^t (t - t^1)^{3/2}\, dt^1$$

$$= -fK^1 D^{3/2}\, \bar{N}\, \gamma\, t^{5/2}$$

or

$$X = 1 - e^{-fK^1 D^{3/2}\, \bar{N}\, \gamma\, t^{5/2}} \qquad \ldots\ (22)$$

where γ is defined by equation 15.

In the absence of knowledge of the type of germ nuclei present and their thermodynamic behavior (information which is virtually non-existent) metallographic evidence must be used

to determine whether equation 21 or 22 is applicable. If the decomposed material has a high nuclei density then equation 21 best describes the decomposition process. If the nuclei density is small then equation 22 is the more appropriate choice.

For the remainder of the derivations only equation 21 will be considered, and γ is assumed to be large. The following treatment can also be applied to equation 22.

Taking the partial derivative of equation 21 with respect to time,

$$\left(\frac{\partial X}{\partial t}\right)_T = 3/2 fKD^{3/2} t^{1/2} (1 - X) \quad . \quad . \quad . \quad . \quad (21a)$$

From absolute reaction rate theory, the diffusion coefficient can be expressed as,

$$D = D_o e^{-Q_D/RT} \quad . \quad . \quad . \quad . \quad (23)$$

where D is the diffusion coefficient, D_o is a frequency factor and Q_D is the experimental activation energy for diffusion. Substituting equation 23 in equation 21a and taking natural logarithms yields,

$$\ln\left(\frac{\partial X}{\partial t}\right)_T = \ln\left(\frac{3fK}{2}\right) + \frac{3}{2} \ln D_o - \frac{3Q_D}{2RT} + 1/2 \ln t + \ln(1 - X)$$

$$. \quad . \quad . \quad . \quad (21b)$$

Taking the partial derivative of equation 21b with respect to T we have,

$$\frac{\partial}{\partial T} \left[\ln\left(\frac{\partial X}{\partial t}\right)_T\right]_X = \frac{-3}{2} \frac{Q_D}{R} \frac{\partial}{\partial T}\left(\frac{1}{T}\right)$$

. .

or $$\frac{\partial\left[\ln\left(\frac{\partial X}{\partial t}\right)_T\right]_X}{\partial\left(\frac{1}{T}\right)} = \frac{-3}{2}\frac{Q_D}{R} \quad \ldots\ldots (21c)$$

since from equation 21, X is a function of the two independent variables T and t. A plot of $\ln\left(\frac{dX}{dt}\right)_T$ for a specific amount transformed versus $\frac{1}{T}$ will give a straight line, the slope of which is equal to $\frac{-3Q_D}{2R}$.

If diffusion-controlled lineal growth (in one direction only) or plate-like growth (in two directions) is involved, then the slopes of the plots $\ln\left(\frac{dX}{dT}\right)_T$ versus $\frac{1}{T}$ are equal to $\frac{-Q_D}{2R}$ and $\frac{-Q_D}{R}$, respectively.

In the more general case where growth in a principal direction is not controlled by diffusion but by atom transfer at the precipitate interface due to orientation effects, then this must be written explicitly into the expression for the precipitate dimension (i.e. D_x, D_y, D_z). If, for example, the growth rates in the y and z directions are orientation controlled at the interface then

$$v = D_x D_y D_z$$
$$= fKD_o^{1/2} e^{-Q_D/2RT} K^{11}\left(e^{-Q_f/RT} - e^{-Q_b/RT}\right)^2 \quad \ldots\ldots (24)$$

since the growth processes in the dimensions D_y and D_z involve atom transfer to and away from the interface, where Q_f and Q_b are defined in Figure 3.

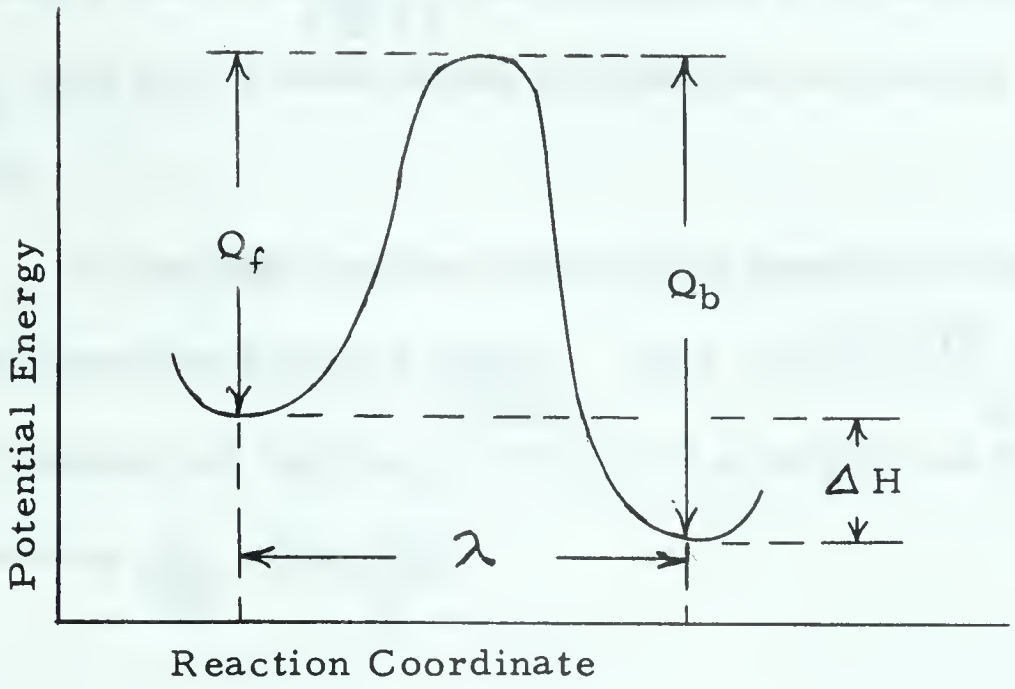

Figure 3. Potential Energy - Reaction Coordinate Plot Representing Atom Transfer at the Precipitate Interface

Equation 24 can be simplified further to

$$v = fKK^{11} D_o^{1/2} e^{-Q_D/2RT} e^{-2Q_f/RT} \left(1 - e^{-\Delta H/RT}\right)^2 \quad . \ . \ . \ . \ (25)$$

where the Q's are taken as the experimental activation energies.

Two extreme cases may be considered: that in which ΔH is small so that the growth of the precipitate in the directions y and z is negligible and

$$K^{11} e^{-2Q_f/RT} \left(1 - e^{-\Delta H/RT}\right)^2 \rightarrow \text{finite constant;} \quad . \ . \ . \ . \ (26)$$

that in which ΔH is very large (corresponding to appreciable growth in the y and z direction) so that equation 26 becomes $K^{11} e^{-2Q_f/RT}$.

In the first case a plot of $\ln\left(\frac{\partial X}{\partial t}\right)_T$ for a specific fraction transformed versus $\frac{1}{T}$ will give a slope equal to $-Q_D/2RT$. In the

second case a plot of $\ln\left(\frac{\partial X}{\partial t}\right)_T$ for a specific fraction transformed versus $\frac{1}{T}$ will give a slope which includes the activation energies Q_D and Q_f.

In the intermediate case ΔH in equation 25 must be evaluated first, then a plot of $\ln\left(\frac{\partial X}{\partial t}\right)_T - \ln\left(1 - e^{-\Delta H/RT}\right)^2_T$ for a specific fraction transferred versus $\frac{1}{T}$ will give a straight line whose slope again involves $\frac{-Q_D}{2R}$ and $\frac{-2Q_f}{R}$.

EXPERIMENTAL

a) Zinc-Aluminum Constitutional Diagram

Although tempering kinetics is the major topic of this thesis, an investigation into the validity of the constitutional diagram was attempted using hot-stage microscopy. The experiment was confined to the zinc - 45 percent aluminum alloy.

In hot-stage microscopy, a sample is polished, etched and then the microstructure is examined at various temperatures. An as-cast sample was heated through the eutectoid temperature and examined for phase changes. The surface wrinkling noticed by Gayler et al[13] was so severe that no constitutional changes could be seen. Another sample was made from an ingot which was homogenized at 400° C. and quenched. This sample was heated to 400° C. and then allowed to cool through the eutectoid temperature, but again, surface deformities hindered microscopic examination. Other samples were given various heat treatments prior to examination, but, in all cases, the surface features were obscured by surface defects. Some samples were examined metallographically.

The technique was abandoned when a literature survey revealed that the present diagram was valid.

b) Tempering Kinetics

Alloys varying from 25 to 90 percent aluminum in zinc were made from vacuum distilled zinc (99.999%) and aluminum

pellets (99.99%). The alloys were melted in an induction melting unit[21] and chill cast, the entire procedure being carried out in an argon atmosphere. The ingots were examined for segregation, homogenized at 400° C. for 48 hours and then quenched. Filings were taken from each ingot, sealed in a thin-walled glass tube containing an argon atmosphere, and heated to 400° C. for homogenization. A number of quenching methods were tried and the method of breaking a thinned glass container in ice-water proved to be the most satisfactory. The oxide layer which is inevitably formed did not affect X-ray diffraction studies.

X-ray diffraction patterns of the quenched alloys were obtained to determine that the α-phase had been completely retained. The quenched powders were resealed in glass containers and tempered to equilibrium at temperatures of 75° C., 100° C., 125° C., and 150° C. X-ray diffraction charts were obtained for the equilibrated powders. The intensity ratios of the two phases, α and β in each equilibrated alloy were obtained by measuring the areas (by planimeter) under the 101 reflection of the c.p.h. (β) phase and the 200 reflection of the f.c.c. (α) phase (Table 1). The two reflections are close to one another so that absorption effects do not contribute much error. The experiment was repeated in triplicate (with duplicate X-ray charts being obtained for each test) and a mean value of intensity ratio was calculated. (Table 1, Appendix 2)

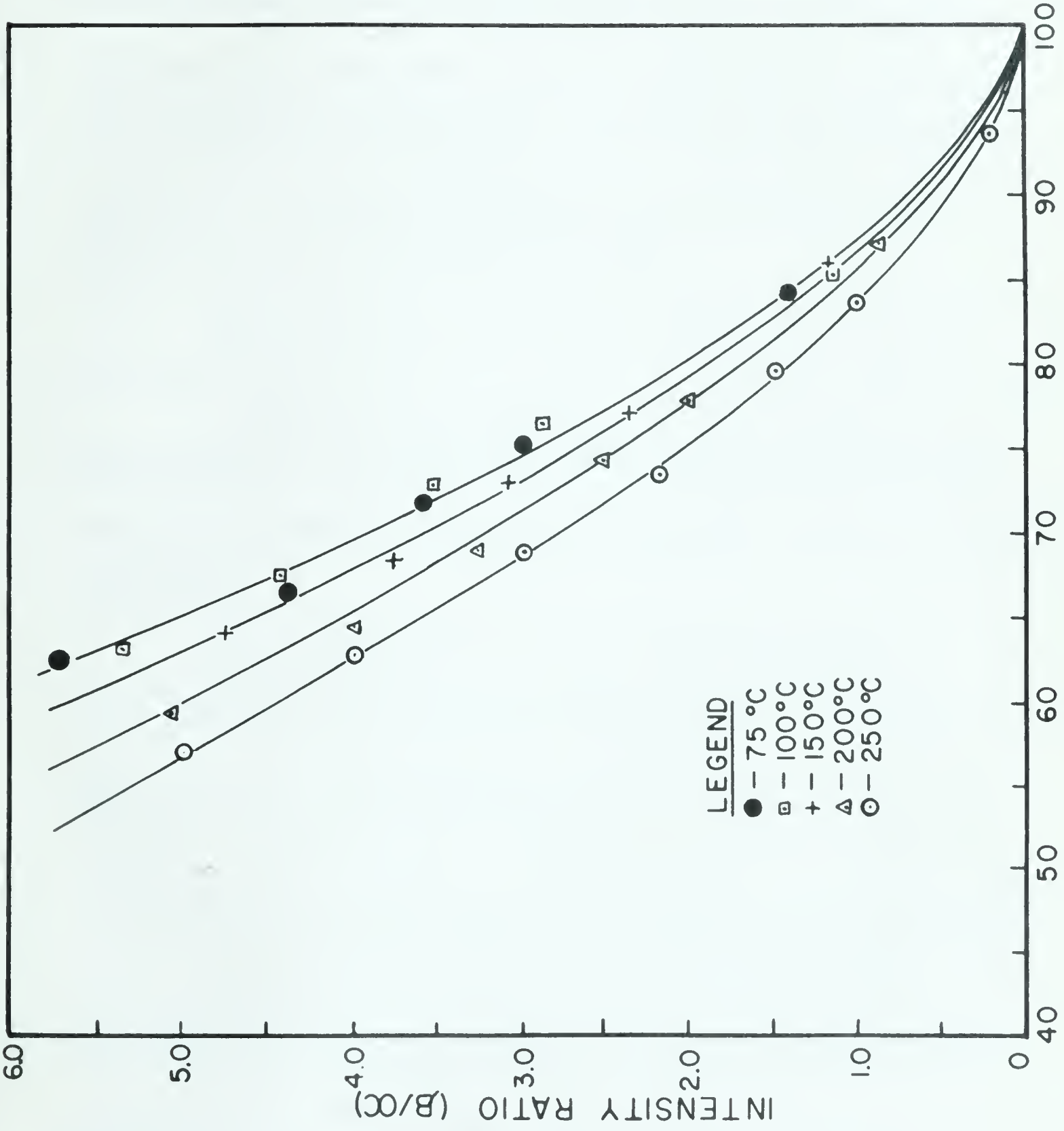

FIGURE 4. CALIBRATION CURVE FOR DETERMINING PHASE RATIOS FROM INTENSITY MEASUREMENTS

The amount of α -phase in each alloy was calculated by applying the lever law to the constitutional diagram. Calibration curves were then made of intensity ratio versus α -phase using temperature as a parameter (Figure 4). Subsequently, for a particular tempering temperature the amount of α -phase present could be deduced simply by measuring the X-ray diffraction intensities for the two reflections mentioned.

The alloys chosen for kinetic studies were 40, 45 and 55 percent aluminum in zinc. Filings from these alloys were homogenized at 400° C. and then quenched. The quenched filings were tempered for measured times and then quenched from the tempering temperature.

Some samples were examined metallographically. The X-ray diffraction intensities of the decomposition products (α and β) were measured and the extent of decomposition was calculated. (Tables 2, 3, 4, in Appendix 2) The time required for the alloy to reach the temperature in question was determined by sealing a thermocouple in a glass tube containing the filings. The tempering time was corrected by the amount of time required to heat the alloy to temperature.

The amount of decomposition was obtained by determining the quantity of β -phase from the measured intensities and the calibration curves. Knowledge of the amount of β in an equilibrated alloy and the quantity of β in the tempered alloy facilitated the

calculation of the fraction of β transformed. (Tables 2, 3, 4, in Appendix 2)

As an example consider the 40 percent aluminum alloy tempered 50 minutes at 150° C. The mean intensity ratio (β/α) is 3.02 which corresponds to 73.0 atomic percent α or 27.0 atomic percent β. The equilibrium amount of β (from the constitutional diagram) is 31.8 atomic percent. The fraction of β transformed is $\frac{27.0}{31.8}$ or 0.74.

The extent of decomposition at room temperature was studied to determine whether any transformation occurred during preparation of the quenched filings for tempering. This was done simply by leaving the quenched alloys in a dessicator and measuring the decomposition at known times. The decomposition was calculated using the calibrated curve for a tempering temperature of 75° C. since the calibration curve for 25° C. was assumed to be approximately coincident with the curve for 75° C. and 100° C.

Also, an alternative procedure was used for studying the decomposition of the 55 percent aluminum alloy at 100° C. The alloy was quenched from 400° C. to 100° C. and then allowed to transform at the latter temperature. The results were compared with the other procedure. The second technique was used to determine whether nucleation was affected by quenching methods.

RESULTS

a) Decomposition Kinetics

Preliminary experimental work provided calibration data which were used to determine the amount of α decomposed at different tempering temperatures and times (Figure 4). The intensity ratios plotted against atomic percent α -phase are a mean value of three tests for which duplicate X-ray charts were obtained.

Transformation-time plots for the 40, 45 and 55 percent aluminum alloys are shown in Figures 5, 6, and 7, respectively. Initially, the transformation proceeds rapidly and then slows until, after tempering approximately 100 minutes, the reaction appears to have stopped.

Transformation rates were obtained by measuring the slopes of the transformation-time curves at specific amounts transformed (30%, 40%, 50% and 60% transformation). The natural logarithm of these rates plotted against the reciprocal of the absolute temperatures (fraction transformed as a parameter), are shown in Figures 8, 9, and 10 for the 40, 45, and 55 percent aluminum alloys, respectively, The straight lines were obtained by balancing the points (area balance), except in the cases where three points lay in a straight line, in which cases the lines were constructed through the three points. The activation energies

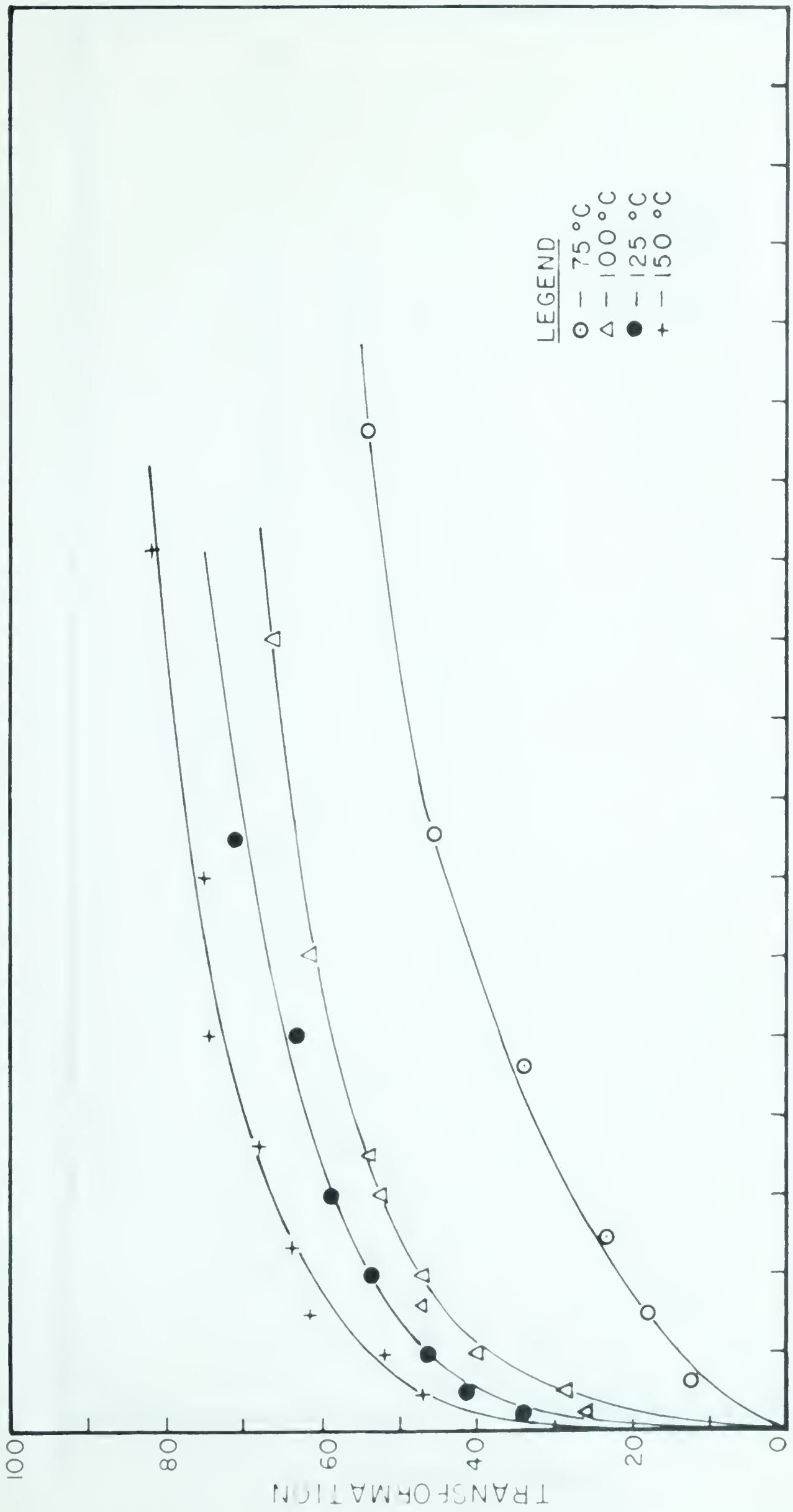

TABLE 5. ISOTHERMAL REACTION CURVES FOR THE 40 PERCENT ALUMINUM ALLOY

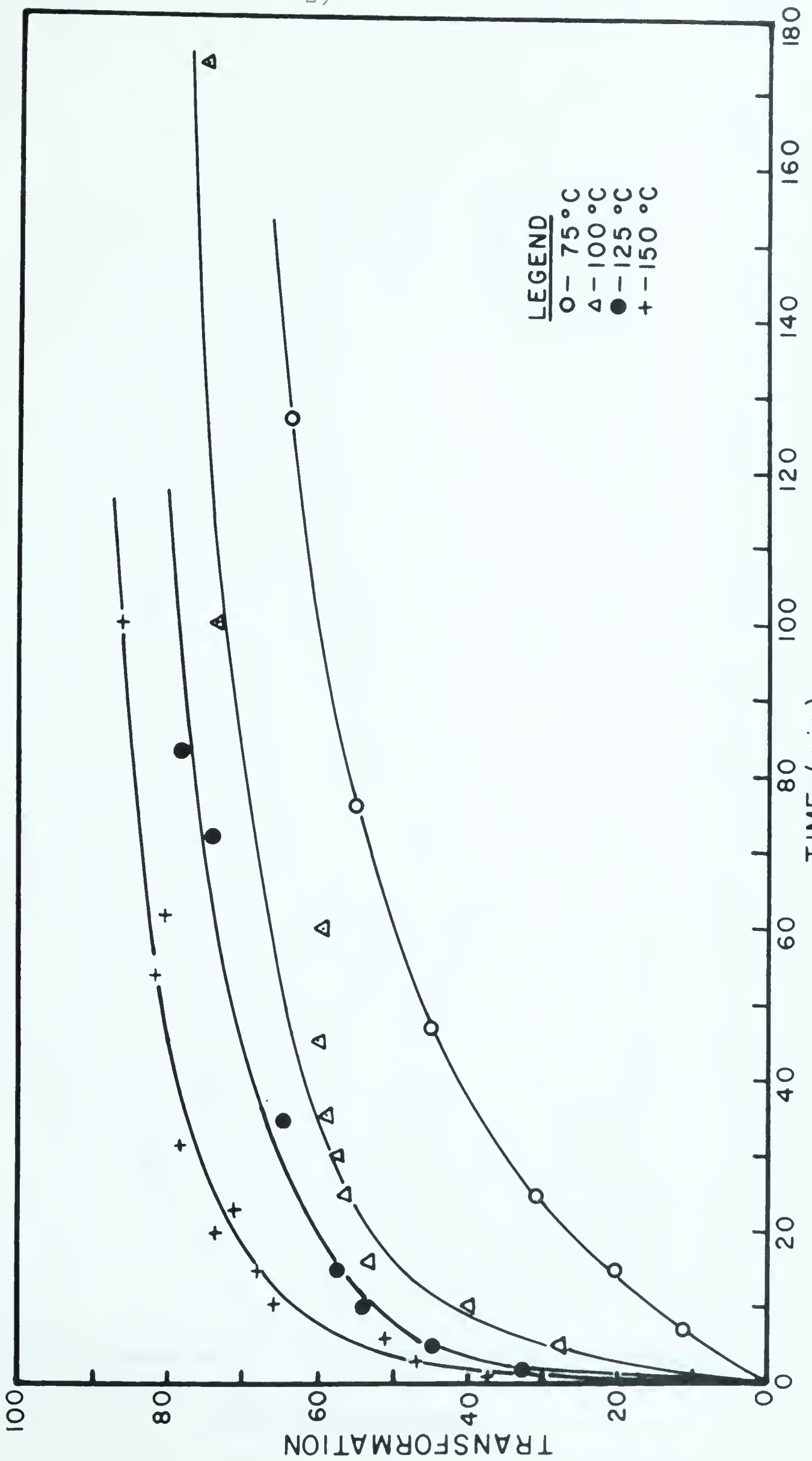

FIGURE 6. ISOTHERMAL REACTION CURVES FOR THE 45 PERCENT ALUMINUM ALLOY

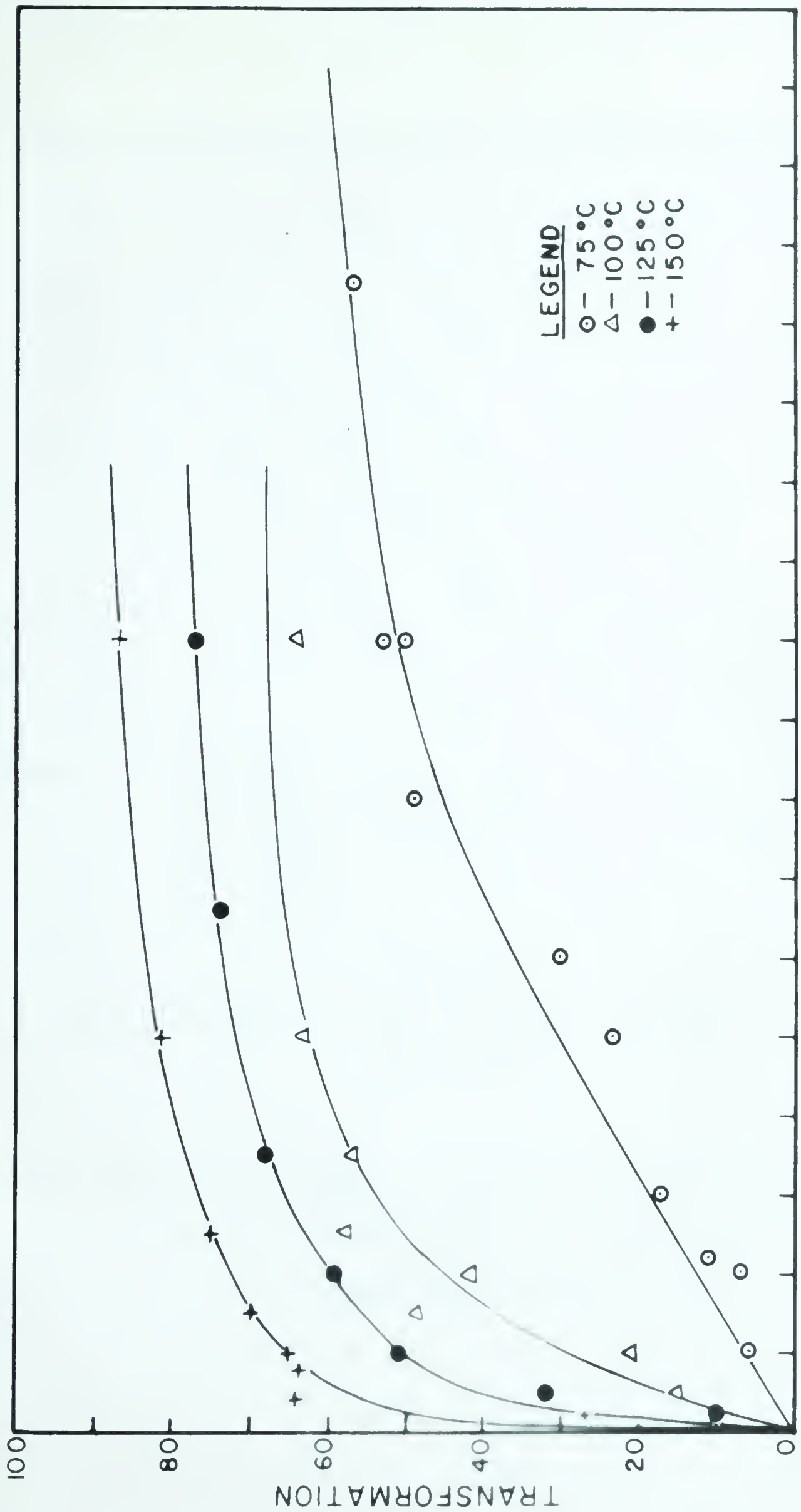

FIGURE 7. ISOTHERMAL REACTION CURVES FOR THE 55 PERCENT ALUMINUM ALLOY

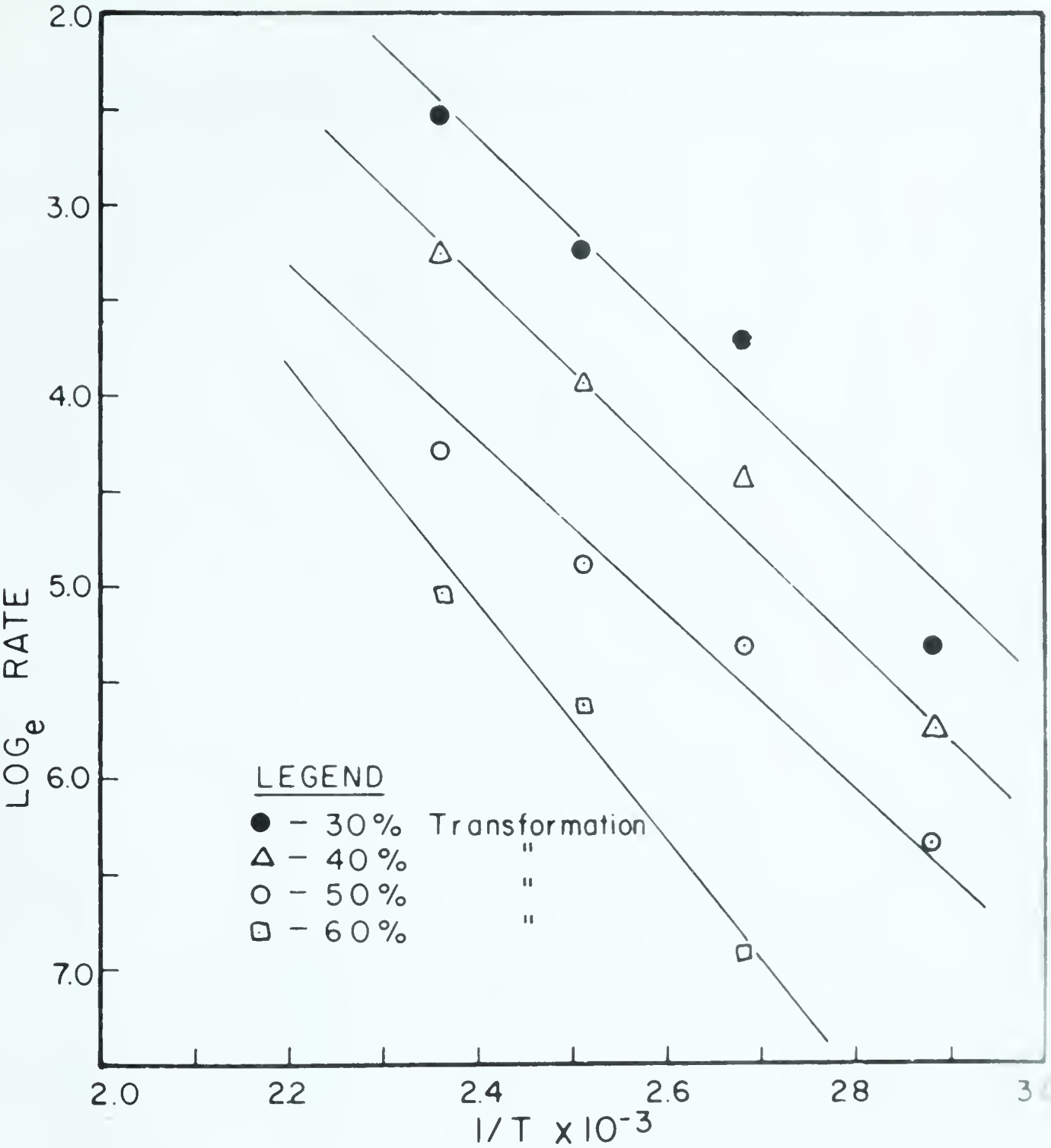

FIGURE 8. GRAPHS OF $\ln\left(\frac{\partial X}{\partial t}\right)_T$ VERSUS 1/T FOR DETERMINATION OF ACTIVATION ENERGY FOR THE 40 PERCENT ALUMINUM ALLOY

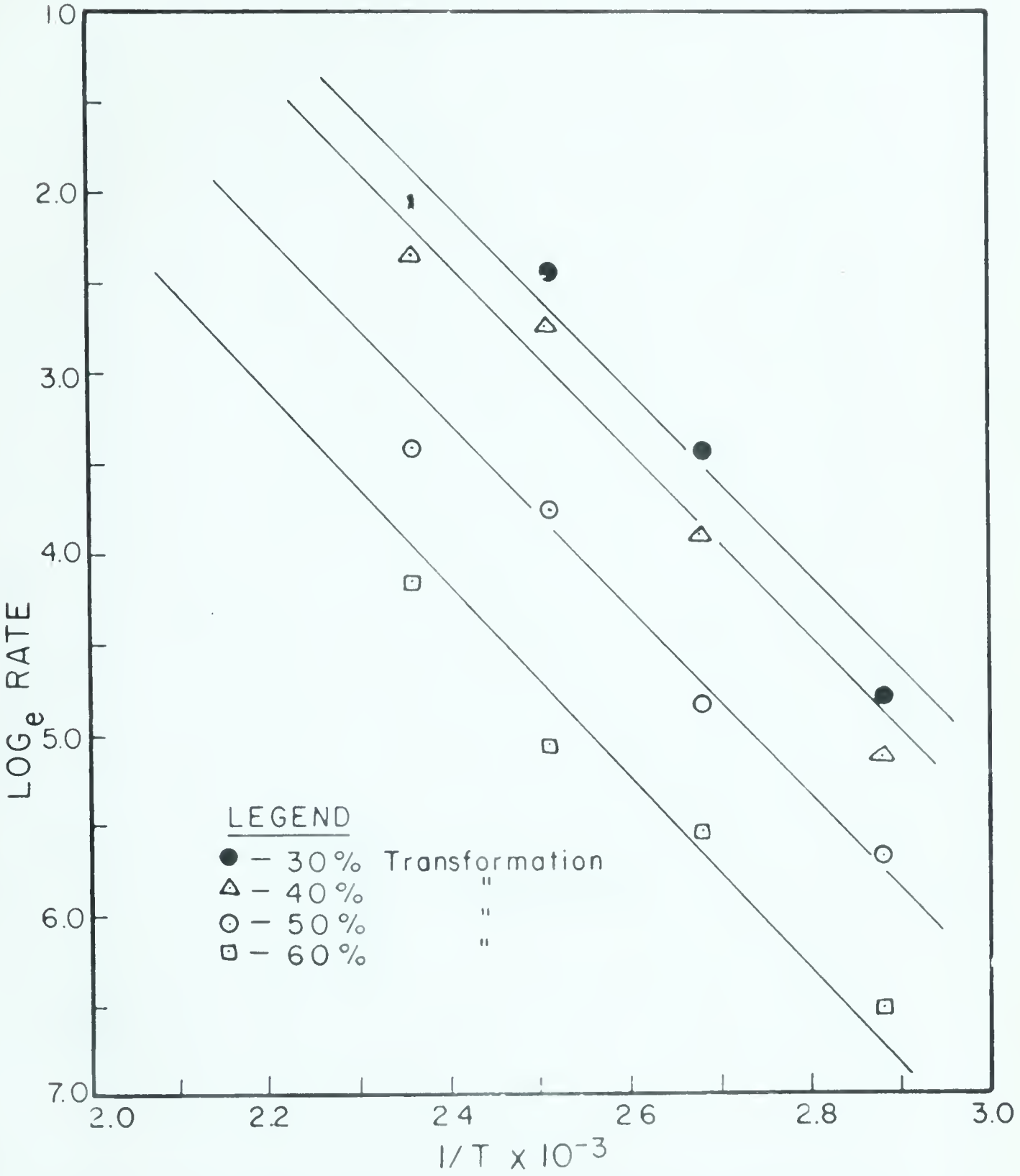

FIGURE 9. GRAPHS OF $\ln\left(\frac{\partial X}{\partial t}\right)_T$ VERSUS 1/T FOR DETERMINATION OF ACTIVATION ENERGY FOR THE 45 PERCENT ALUMINUM ALLOY

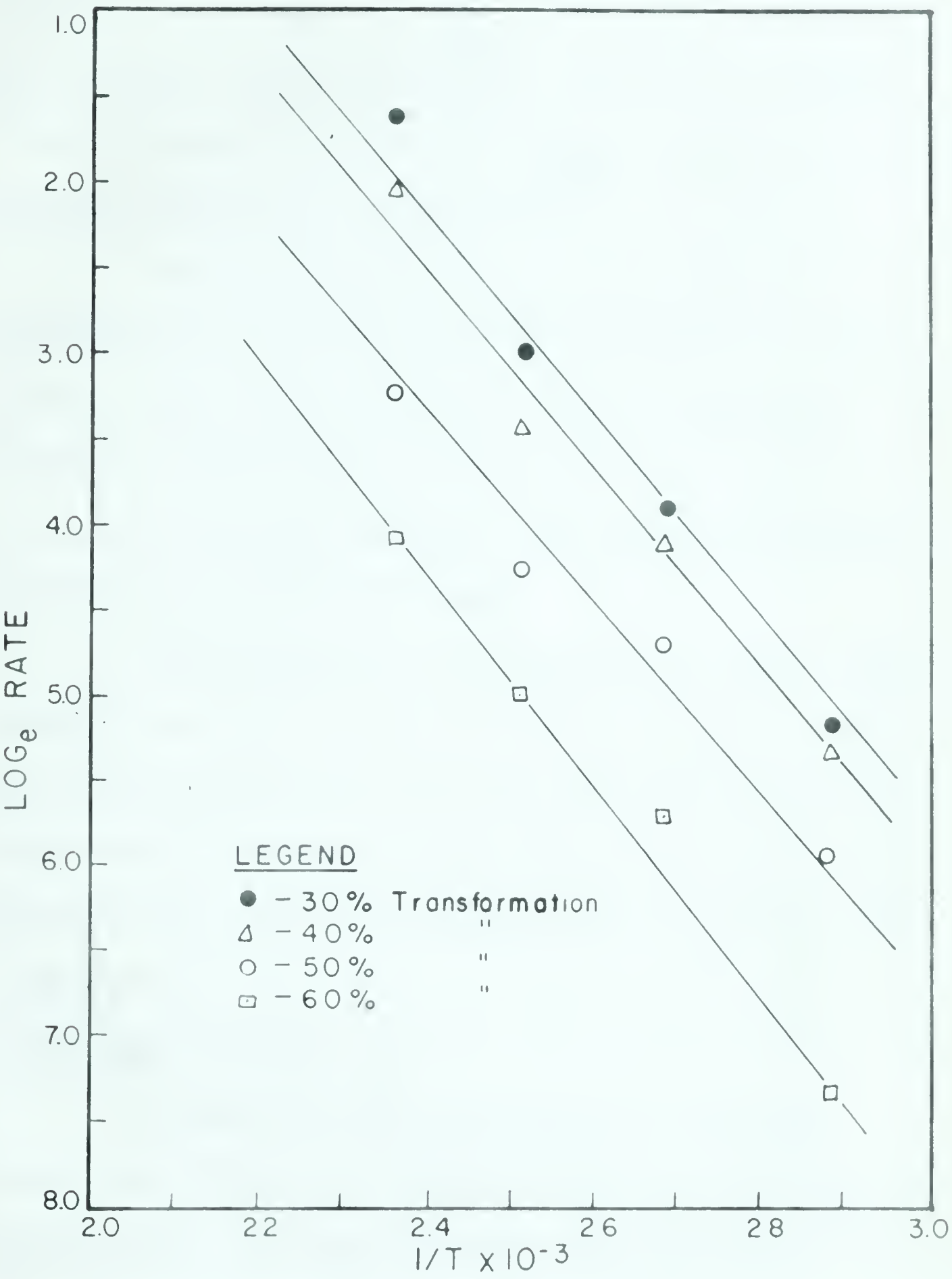

FIGURE 10. GRAPHS OF $\ln\left(\frac{\partial X}{\partial t}\right)_T$ VERSUS 1/T FOR DETERMINATION OF ACTIVATION ENERGY FOR THE 55 PERCENT ALUMINUM ALLOY

calculated from the slopes (i. e. $-\frac{Q_D}{2R}$ for lineal growth) of these lines are listed in Table 5 (Appendix 2). The activation energies for the alloys vary between 18.6 and 25 $\frac{kcal}{mole}$, depending upon the composition and amount of transformation.

The results of the delayed quench technique (i. e. quenching the alloy from the homogenization temperature to the tempering temperature) are indicated in Table 4 (Appendix 2) by asterisks. There was no appreciable difference between the data obtained using either technique. This suggests the nucleation is unaffected by quenching techniques.

The decomposition of the metastable α-phase at room temperature does not proceed sufficiently fast to affect the constitution of the quenched alloys during the preparation for tempering. Furthermore, the decomposition rate of the metastable α at room temperature decreases as the aluminum content increases. (Table 6, Appendix 2)

b) Evaluation of Results

Although the error in each test can be discussed quantitatively, the error in activation energy may be discussed only qualitatively. The activation energy calculation involves not only the use of the calibration curves but also slopes of the transformation-time curves. Hence, the calculation involves the use of representative plots plus a number of mathematical calculations.

An error which is inherent in all work of this type is inhomogeneity in cast ingots. Although the ingots were homogenized at 400° C. for 48 hours a uniform composition throughout the ingot may not have been produced. The filings would then vary constitutionally from sample to sample. This error, however, would be small because segregation affects caused by the technique used are not appreciable.

In the X-ray diffraction studies, errors may arise at the beginning of transformation since the presence of less than five percent of one phase is not easily detected. As the amount of this phase increases, however, the assessment of phase ratios is reasonably accurate.[22] Further, since triplicate tests were made and each of these examined in duplicate, the error in the mean value for the intensity ratio is considerably reduced. The calibration curves were plotted by weighing the data proportionately and are representative of the mean values of intensity ratios. The error in the data is thus further reduced.

The error in temperature measurement is ± 2° C. and does not contribute much error in the activation energy. The error in time measurement varies with tempering time. Since corrections were made to the time measurements, the probable errors are proportionately large for short times but small for long times.

However, the probable errors in time measurements are somewhat reduced since duplicate tests were made.

Other errors may arise in measurements of the amounts transformed from the calibration data. Conceivably, significant errors would result in these measurements if the intensity ratios of the tempered alloys were appreciably in error. The best fit curve for the transformation-time relations is representative of many points and should reduce the error in every point. The error in measurement of the slope of the transformation-time curve is comparatively small.

Another source of error in the activation energy arises through determination of the best-fit line in the plots of ln(rate) versus $\frac{1}{T}$. Since the method of balancing areas was used, a large error in every point could cause considerable error in the activation energy. However, since the fraction transformed is a parameter, a line balanced incorrectly can be adjusted to fit the trend of most of the lines.

c) Microstructures

Figure 11 shows a photomicrograph of the 40 percent aluminum alloy which was tempered for 15 minutes at 150° C. The matrix material consists essentially of α-phase while the dark areas indicate the beginning of β growth. Although it is not

too evident the precipitated β-phase appears lineal (the ratio of length to width is large) illustrating preferred growth in certain crystallographic directions. The tiny particles in the α-phase are either the cross-sections of the precipitates or are the beginning of more nuclei growth.

The microstructure of the 40 percent alloy tempered 1000 minutes at 150° C. is shown in Figure 12. Evidence that the growth of a precipitate occurs preferentially along certain crystal directions is well illustrated by this microstructure. The diffusion of the principal component (zinc) must be easier along certain planes, or alternatively, diffusion into the precipitate from other directions may be retarded by unfavourable atomic configurations at the interface. Either of the possibilities would promote growth of the β-phase in preferred directions.

Figure 13 illustrates the microstructure of the 40 percent alloy tempered 2000 minutes at 75° C. Comparison with Figure 11 shows the effect of tempering temperature on precipitate size. The precipitate of the alloy tempered at 75° C. is much finer although the number of precipitates per unit area has increased. However, the shape of the β-precipitate is similar to that shown in Figure 11 and suggests one dimensional growth at lower temperatures.

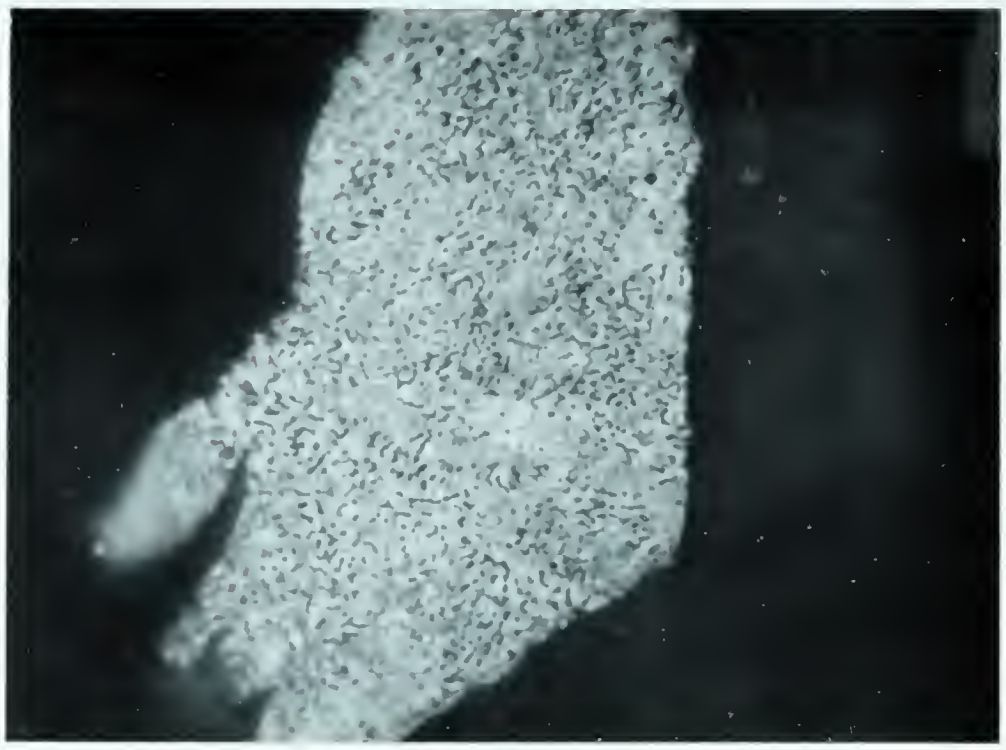

Figure 11. Photomicrograph of Zn-40% Al Tempered 15 Minutes at 150° C - Mag. 1700X
Etchant: Etched 4 seconds in 70% HNO_3

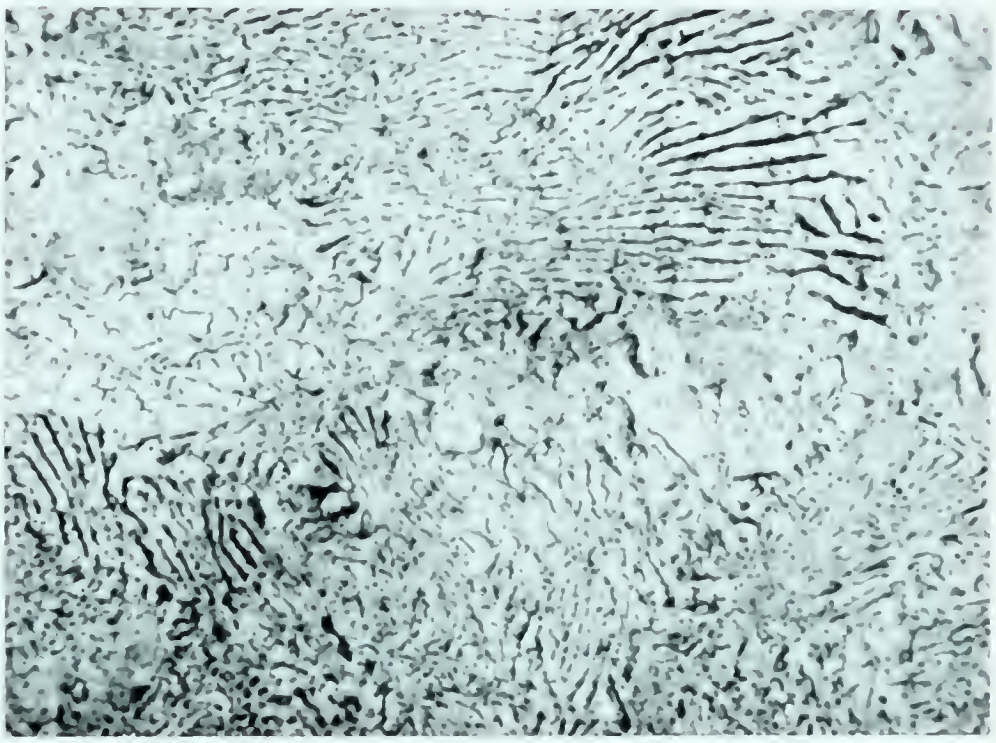

Figure 12. Photomicrograph of Zn-40% Al Tempered 1100 Minutes at 150° C - Mag. 1700X
Etchant: Etched 4 seconds in 70% HNO_3

The 55 percent aluminum alloy tempered 1000 minutes at 125° C. is shown in Figure 14. Despite the fact that the precipitate is less in amount and is more widely dispersed, the shape is similar to that in the other microstructures. The dispersion of the β decreases the impingement and interaction effects, and consequently a larger fraction of the β transforms before these effects become appreciable.

Figure 13. Photomicrograph of Zn-40% Al Tempered 2000 Minutes at 75° C. - Mag. 1700X
Etchant: Etched 4 seconds in 70% HNO_3

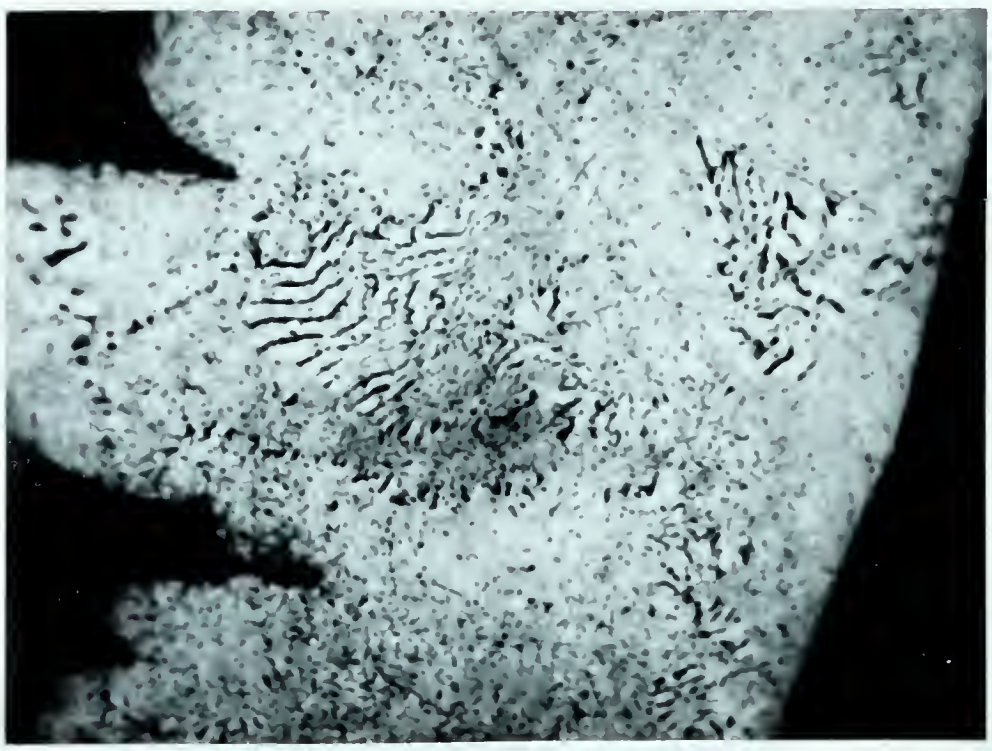

Figure 14. Photomicrograph of Zn-55% Al Tempered 1000 Minutes at 125° C. - Mag. 1700X
Etchant: Etched 4 seconds in 70% HNO_3

DISCUSSION

The rate equations derived from absolute reaction rate theory and presented in this thesis illustrate the relationship between the variables affecting the decomposition rate of a metastable phase in alloys. Examination of these rate equations shows how the nucleation parameter and the growth parameter, being explicitly defined, affect the value of the activation energy. Further, the experimental data is more directly treated than in alternative methods.

The equation that was used by Cohen and other investigators does not define the variables explicitly, but groups all of them into a modified rate constant. This treatment involves a determination of an "n" value (i. e. m + 1) that is used to calculate an overall activation energy -- the meaning of which is vague.

Equation 21 lends itself to easy manipulation and gives a straightforward result provided that the variables are chosen to accommodate the preferred growth directions.

The importance of microstructural examination to determine the growth and nucleation characteristics of the precipitating phase cannot be over emphasized. The shape of the precipitate indicates whether growth occurs preferentially in any one direction or directions, or is equal in all directions. If the precipitate

shape is complex, equations similar to equation 25 must be used. The variation in growth is expressed by activation energies that correspond to the factors controlling the growth in the different directions. In such decomposition studies -- where the precipitating phase is controlled by factors other than uni-dimensional diffusion -- the treatment becomes complicated. In reality, however, the shape of the precipitate is usually spheroidal, plate-like or lineal -- which enables a direct application of equation 21.

If a treatment similar to Cohen's is used an n value, which is determined by growth type, must be calculated. However, the use of log log f(X) versus log (t) plots to evaluate n is subject to errors, because any effects due to interaction of diffusion fields are masked. (Appendix 1) Further, any subtleties in a direct f(X):t variation, tend to be lost in a plot of log log f(X) versus t.

It is therefore more desirable to treat experimental data by calculating rates from slopes of transformation-time curves. Before activation energies are calculated, an investigation of the precipitate form must be made to determine whether equation 21 applies directly (i. e. three dimensional growth by diffusion) or requires modification to account for the growth and nucleation mechanisms.

In this study of zinc-aluminum alloys, the microstructures revealed a nucleation rate corresponding to equation 18 and a pre-

cipitate that was decidedly lineal. Therefore equation 21, modified for the one-dimensional case, may be used.

The activation energies in this study increase with aluminum content of the alloys with the exception of the activation energy for the 40 percent aluminum alloy at 60 percent transformation. This may be due to impingement effects for higher amounts transformed. The increase in activation energies with aluminum content agrees with the work of Hilliard, Averbach and Cohen[23] for the self-diffusion of zinc in zinc-aluminum alloys. Hilliard et al found that the activation energy increased slightly with aluminum content in the composition range studied in this thesis. There is also an increase in activation energy as decomposition proceeds and this is due to the reduced concentration gradient arising between the alloy and the precipitate interface that occurs as the growth of the precipitate advances.

A radical change in activation energy as transformation proceeds would illustrate the effect of impingements and interaction of diffusion fields on precipitate growth. In the alloys studied the amount of precipitate and the number of nucleation sites were large -- which suggests that the interaction effects would be considerable after long tempering times. This complication is avoided by using the data at short tempering times. For alloys in which the

quantity of precipitate is small (as in mild steels precipitating carbides), the nucleation sites are widely separated from one another so that the interaction between precipitates is small and consequently application of the Cohen method gives good results.

An error in the activation energy may be caused by experimental technique, manipulation of data, or it may be inherent to the rate equation. The assumption that the diffusion frequency and activation energy are independent of temperature is a good approximation if the temperature range is small. Consequently, this assumption should not affect the results in this thesis significantly. Furthermore, the choice of lineal growth appears to be a reasonable assumption.

The diffusion model requires counter diffusion of zinc and aluminum. The controlling mechanism is the self-diffusion of zinc in the α-matrix (intrinsic diffusivity of zinc[24]). Whether the counter diffusion of zinc is substitutional or vacancy (for vacancies may be present in the α-phase) is of no concern in the present work. The activation energy given in the literature[23] for the self-diffusion of zinc in zinc-aluminum alloys is between 23.7 and 24.6 kcal./mole for the compositions studied. The activation energies determined by these tempering investigations are in the range 18.6 to 25.0 kcal./mole, which indicates the validity of the diffusion model and the rate equation.

CONCLUSIONS

(a) The rate equation (21) derived in this thesis is in general applicable to all types of growth mechanisms. For any particular growth mechanism the equation can be modified after preliminary microstructural examinations have indicated the growth characteristics of the precipitate. Usually, the precipitate form is simple (i. e. lineal, plate-like or spheroidal) and consequently the activation energy calculations are straight forward. In the more complex cases, where growth in some directions are orientation controlled, activation energies can be calculated provided that relevant thermodynamic variables are known.

(b) The controlling mechanism for the decomposition rate of metastable α in zinc-aluminum alloys is the self-diffusion of zinc in the α-matrix. The term "self-diffusion" of zinc, as applied to aluminum-zinc alloys, means that zinc has an "intrinsic" diffusivity which differs from that of aluminum (i. e. the movement of a zinc atom does not necessarily depend on the corresponding movement of an aluminum atom). The growth of the β precipitate occurs along preferred crystallographic directions by a diffusion process. The growth in the other two directions is controlled by orientation effects which prevent the deposition of zinc atoms on the precipitate interface.

The activation energies for the self-diffusion of zinc in zinc-aluminum alloys, in the range of compositions studied, are between 23.7 and 24.6 kcal./mole. Since the activation energies for the decomposition studies are between 18.6 and 25.0 kcal./mole and comparable to the activation energies given above, the proposed diffusion model is valid.

(c) Interactions of diffusion fields and impingements are significant when the amount of precipitate is large or when nucleation sites are numerous. Interactions and impingements account for the sluggish approach to final equilibrium.

BIBLIOGRAPHY

1. A. S. M. Metals Handbook, 1956, p. 1167

2. Roberts, C. S., Averbach, B. L., and Cohen, M., Trans. A. S. M., 1953, Vol. 45, p. 576

3. Johnson, W. A., and Mehl, R. F., Trans. AIME, 1939, Vol. 135, p. 416

4. Owen, W. S., Trans. AIME, 1954, Vol. 46, p. 812

5. Polonis, D. H., and Parr, J. G., Acta Met., 1955, Vol. 3, p. 307

6. Rosenhain, W., and Archbutt, S. L., Phil. Trans. Roy. Soc. 1911 (A), Vol. 211, p. 315

7. Bauer, O., and Vogel, R., Internat. Z. Met., 1916, Vol. 8, p. 101

8. Hanson, D., and Gayler, M. L. V., J. Inst. Metals, 1922, Vol. 27, p. 267

9. Tanabe, T., J. Inst. Metals, 1924, Vol. 32, p. 415

10. Isihara, T., J. Inst. Metals, 1925, Vol. 33, p. 73

11. Fink, W. L., and Willey, L. A., Trans. AIME, 1936, Vol. 122, p. 244

12. Owen, E. A., and Pickup, L., Phil. Mag., 1935, Vol. 20, p. 761

13. Gayler, M. L. V., and Sutherland, E. G., J. Inst. Metals, 1938, Vol. 63, p. 123

14. Elwood, E. C., J. Inst. Metals, 1940, Vol. 66, p. 87

15. Elwood, E. C., J. Inst. Metals, 1951-52, Vol. 80, p. 217

16. Rhines, F. N., Phase Diagrams in Metallurgy, McGraw-Hill, 1956, p. 76

17. Kirkaldy, J. S., and Youdelis, W. V., AIME, 1958, Vol. 212, p. 833

18. Youdelis, W. V., and Colton, D. R., to be published

19. Zener, C. J., J. App. Phys., 1949, Vol. 20, p. 950

20. Avrami, M., J. Chem. Phys., 1939, Vol. 7, p. 1103

21. Yurko, G. A., Whittaker, D. A., Parr, J. G., to be published

22. Parr, J. G., Research, 1953, Vol. 6, p. 375

23. Hilliard, J. E., Averbach, B. L., and Cohen, M., Acta Met., Feb. 1959, Vol. 70, p. 86

24. Darken, L. S., Trans. AIME, 1948, Vol. 175, p. 184

APPENDICES

APPENDIX I

ALTERNATIVE METHODS FOR CALCULATING ACTIVATION ENERGIES

The treatment, used by Cohen and other investigators mentioned in this thesis, for calculating an activation energy of decomposition cannot be rejected without justification. The purpose of this appendix is to show that their data gives results that cannot be completely explained.

Cohen developed a rate equation which is similar to the one derived in the theory section of this thesis. Like Avrami, Cohen has suggested that active nuclei are present before, or at, the beginning of tempering. The same hypothesis is applied to martensitic transformations, in which it is suggested that embryos exist in the austenite and become active martensitic nuclei at lower temperatures.

If the experimental data for the 40 percent aluminum alloy (Table 2 in Appendix 2) is plotted with fraction transformed as the ordinate and logarithm of time as the abscissa, the curves produced are typical "S" curves (Figure 1).

In the normal treatment of experimental data, equation 2 is used in the form,

$$\log_{10}\log_{10}\left(\frac{1}{1-X}\right) = \log_{10}\frac{K}{2.3\,(m+1)} + (m+1)\log_{10} t$$

plot of $\log_{10} \log_{10}\left(\frac{1}{1 - X}\right)$ versus $\log_{10} t$ should yield a straight line with intercept on the ordinate of $\log_{10} \frac{K}{2.3\,(m+1)}$ and slope $(m + 1)$, Figure 2. In the Arrhenius equation, $k = Ae^{-Qt/RT}$, and a plot of lnk versus $1/T$ yields a line whose slope is Q_t/R. Hence a plot of $\log \frac{K}{2.3(m+1)}$ versus $1/T$ yields a line of slope Q_k/R, Figure 3. It is then assumed that the activation energy, Q_k, is converted into a true activation energy, Q_t, by dividing by $(m + 1)$, which then gives the correct units with respect to time for K. This, however, has not been rigorously justified.

An inspection of Figure 2 shows that it is difficult to construct a representative curve through the points, and also illustrates the deviation of the curves from linearity after approximately one half the β has transformed. The linearity cannot be justified and as a result the intercepts and the slopes are probably in error. Therefore a plot of $\log \frac{K}{2.3(m+1)}$ versus $1/T$ will yield an activation energy Q_k which has doubtful significance. The value of $(m + 1)$ is 0.32 and the corresponding activation energy is 10.7 kcal./mole.

An alternative procedure may be employed wherein the transformation-log time plots are used to determine the times required for a specific fraction transformed at the different temperatures. Since it is assumed that $K = K_o\, e^{-Q_k/RT}$ substitution into the integrated forms of equation 1 yields

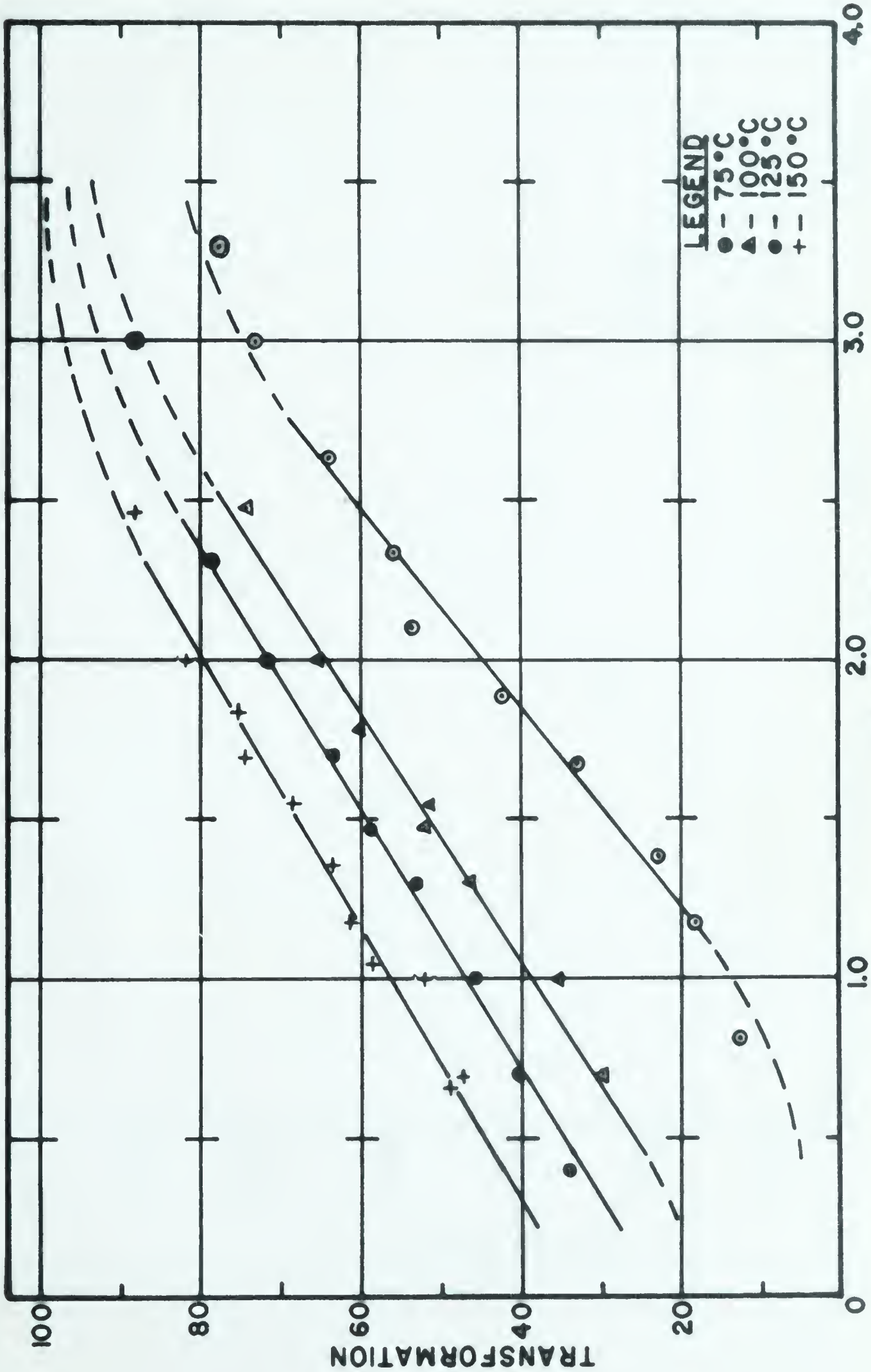

FIGURE 1. PLOT OF TRANSFORMATION VERSUS LOG TIME FOR 40 PERCENT ALUMINUM ALLOY

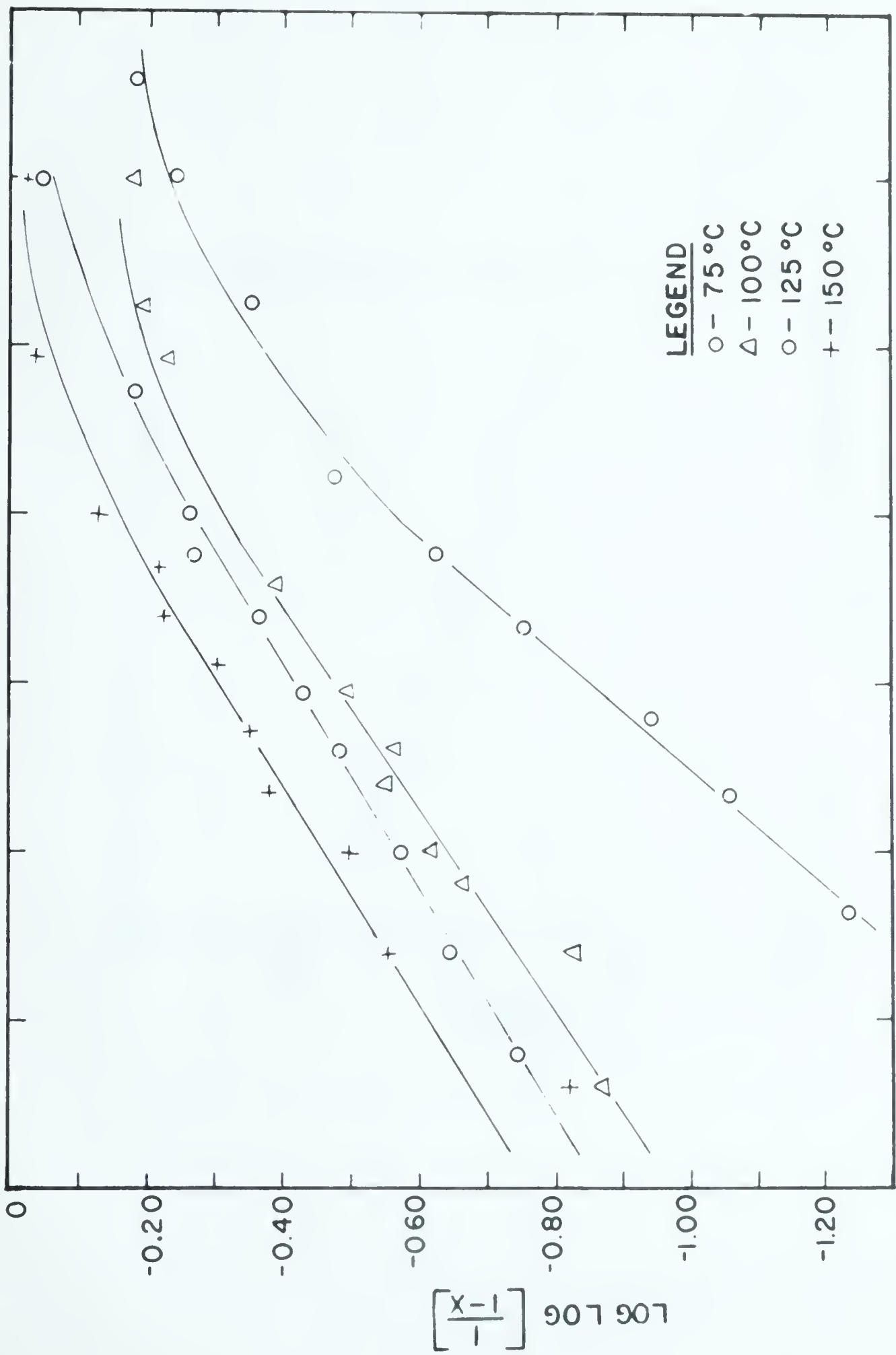

FIGURE 2. PLOT OF LOG $\frac{1}{1-X}$ VERSUS LOG TIME FOR THE DECOMPOSITION OF X IN THE 40 PERCENT ALUMINUM ALLOY

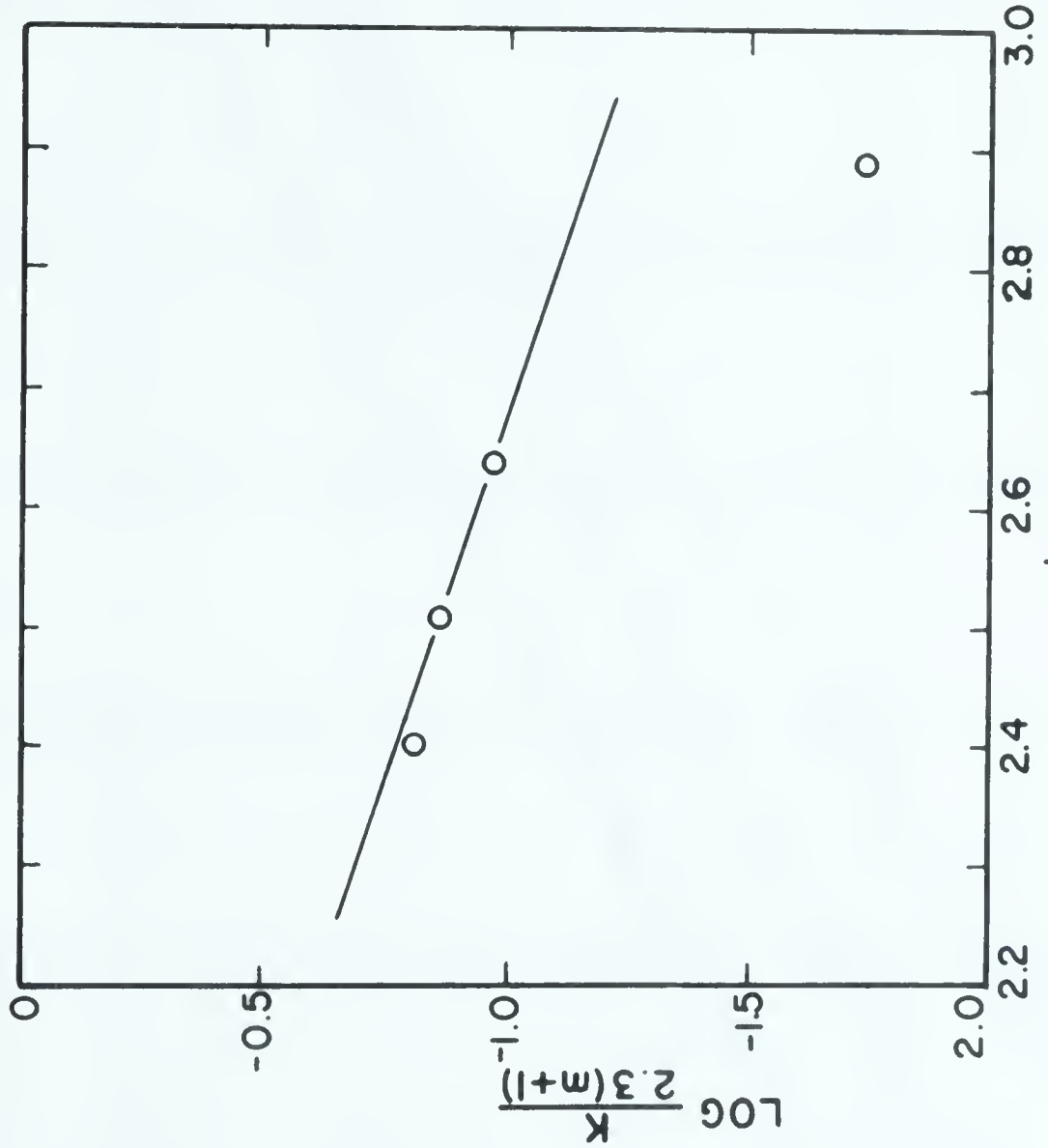

FIGURE 3. PLOT OF LOG LOG $\frac{K}{2.3(m+1)}$ VERSUS $\frac{1}{T}$ FOR THE DECOMPOSITION OF K IN THE 40 PERCENT ALUMINUM ALLOY

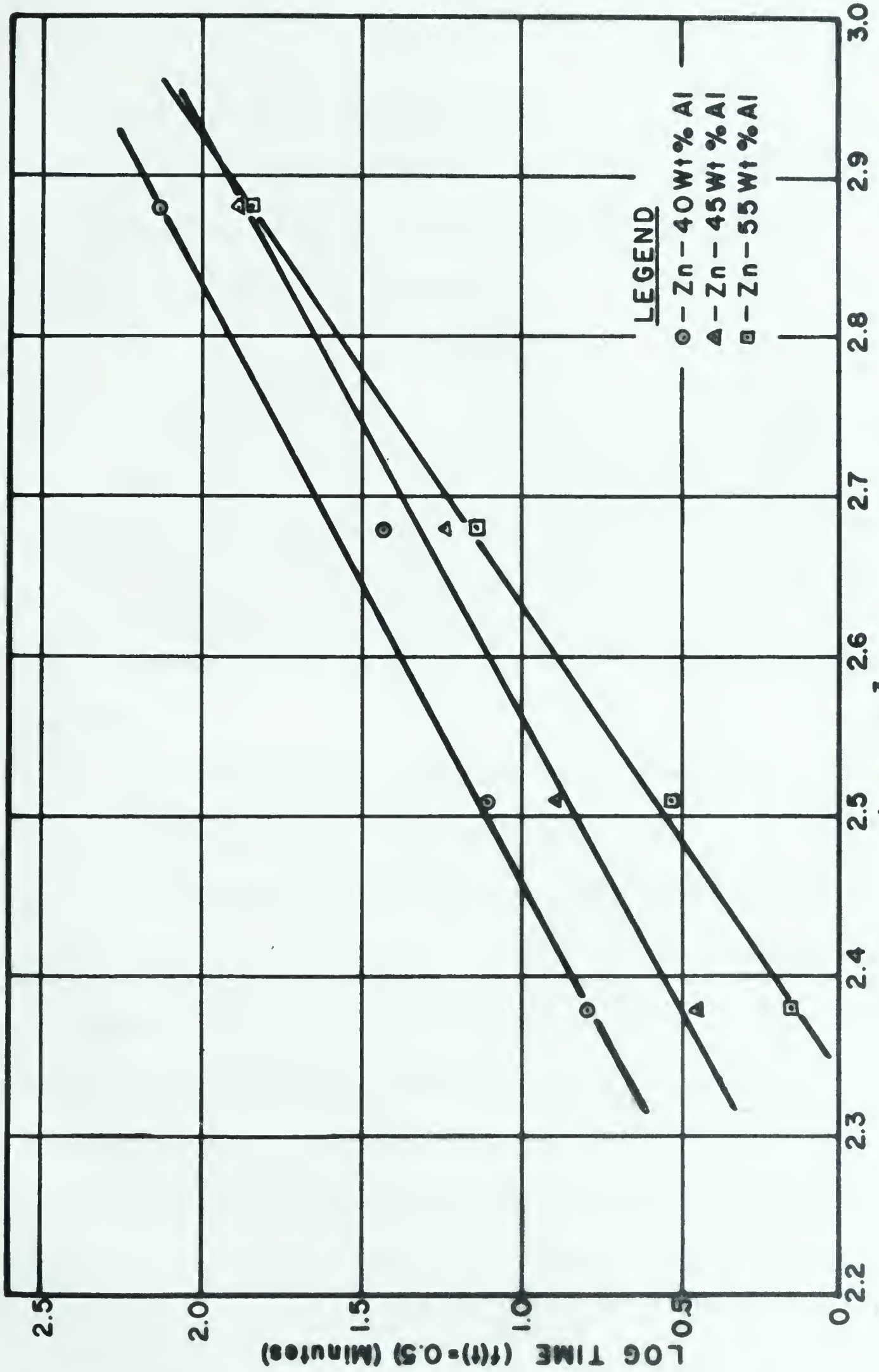

FIGURE 4. PLOT OF LOG TIME FOR A SPECIFIC AMOUNT TRANSFORMED VERSUS 1/T FOR THE DECOMPOSITION OF X IN THE 40, 45, AND 55 PERCENT ALUMINUM ALLOYS

$$K_o\, e^{-Q_k/RT} = \frac{-(m+1)(1-X)}{t^{m+1}}$$

Assuming K_o is a frequency factor for a first order reaction and that m is constant, then for a specific amount of transformation the above equation can be manipulated to

$$\log t = \frac{Q_k}{2.3\,(m+1)RT} + \text{constant}$$

Therefore a plot of log t versus 1/T yields a line of slope $\frac{Q_k}{2.3(m+1)RT}$ if the activation energy is independent of temperature (Figure 4). Therefore, the true activation Q_t is simply $\frac{Q_k}{m+1}$ or 2.3R multiplied by the slope of the line. The activation energies of the 40, 45, and 55 percent aluminum alloys were 12.2, 12.4, and 15.4 kcal./mole, respectively.

For this approach, calculation of an n value is not necessary and an activation energy is obtained directly. However, since a transformation-log time curve is used to obtain data for the plot of $\log_{10} t$ versus 1/T plot, the results are in error since the linear portion of the curve cannot be drawn accurately. The effects of interacting diffusion fields and impingements cause the curve to deviate from linearity after only a fraction of the transformation. Inevitably the curve is drawn through the best-fit data where these effects are proportionately high, thus leading to values of activation energy which cannot be completely explained.

APPENDIX II

SUMMARY OF SIGNIFICANT EXPERIMENTAL DATA AND RESULTS

TABLE I. X-RAY CALIBRATION FOR DETERMINING PHASE RATIOS FROM INTENSITY MEASUREMENTS

	75° C.		100° C.		125° C.		150° C.		200° C.		250° C.	
Alloy Wt% Al	At.% α	Area Ratio β_{101}/α_{200}	At.% α	Area Ratio β_{101}/α_{200}	At.% α	Area Ratio β_{101}/α_{200}	At.% α	Area Ratio β_{101}/α_{200}	At.% α	Area Ratio β_{101}/α_{200}	At.% α	Area Ratio β_{101}/α_{200}
25	45.5	-	45.9	-	46.2	-	46.3	9.16	46.6	7.61	49.4	6.22
30	51.9	9.90	52.4	9.61	52.7	9.13	53.0	8.26	53.3	6.38	56.8	5.00
35	57.2	6.89	57.8	6.83	58.1	6.58	58.4	6.15	58.9	4.83	62.8	3.99
40	62.5	5.70	63.1	5.35	63.4	5.16	63.8	4.73	64.3	3.75	68.8	3.01
45	66.7	4.38	67.4	4.40	67.8	4.10	68.2	3.72	68.9	3.06	73.7	2.18
50	71.9	3.53	72.7	3.49	73.0	3.38	73.4	3.07	74.2	2.48	79.5	1.50
55	75.4	2.95	76.2	2.87	76.6	2.72	77.0	2.35	78.0	2.00	83.5	1.02
70	84.3	1.45	85.2	1.13	85.7	1.33	86.1	1.21	87.3	0.87	93.7	0.27
90	96.3	0.09	97.2	-	-	-	-	-	-	-	-	-

Note: Atomic percent α-phase was calculated from the constitutional diagram.
The area ratios are mean values representing duplicate studies on three tests.

TABLE 2. DATA FOR DECOMPOSITION OF α IN ZINC-40% ALUMINUM

Temp.	Time (min.)	Log Time	Area Ratio β_{101}/α_{200}	%α From Calibration Curve	%β	X=Fraction Transformed x100	$\text{Log}_{\frac{1}{1}}\text{Log}\left[\frac{1}{1-X}\right]$
75°C.	Quenched	-	0	100	0	0	-
	6.5	0.813	0.24	95.3	4.7	12.5	-1.237
	15	1.176	0.38	93.2	6.8	18.1	-1.061
	24.5	1.389	0.49	92.0	8.0	22.8	-0.943
	46.5	1.667	1.02	87.5	12.5	33.3	-0.752
	75.5	1.878	1.43	84.2	15.8	42.2	-0.624
	126.5	2.102	2.10	79.8	20.2	53.8	-0.474
	216	2.334	2.23	79.0	21.0	56.0	-0.448
	423.5	2.627	2.75	76.0	24.0	64.0	-0.352
	1000	3.000	3.40	72.5	27.5	73.3	-0.241
	2000	3.301	3.76	70.8	29.2	77.8	-0.185
100°C.	Quenched	-	0	100	0	0	-
	2	0.303	0.72	90.2	9.8	26.6	-0.870
	5	0.699	0.78	89.0	11.0	28.4	-0.836
	8	0.903	1.23	85.6	14.4	39.0	-0.668
	10	1.000	1.35	84.9	15.1	40.9	-0.640
	16	1.204	1.71	82.3	17.7	47.9	-0.547
	20	1.303	1.63	82.8	17.2	46.6	-0.566
	30	1.477	1.95	80.7	19.3	52.3	-0.492
	60	1.778	2.51	77.4	22.6	61.2	-0.386
	100	2.000	3.33	73.0	27.0	73.2	-0.243
	300	2.477	3.40	72.5	27.5	74.5	-0.227
	420	2.623	3.57	71.4	28.6	77.5	-0.188
	1000	3.000	3.54	71.3	28.7	78.0	-0.182
125°C.	Quenched	-	0	100	0	0	-
	2.5	0.398	0.94	87.5	12.5	34.2	-0.740
	5	0.699	1.22	85.1	14.9	40.7	-0.644
	10	1.000	1.42	83.2	16.8	46.0	-0.572
	20	1.303	1.90	80.5	19.5	53.2	-0.482
	30	1.477	2.23	78.5	21.5	58.8	-0.425
	50	1.699	2.50	76.8	23.2	63.3	-0.361
	76	1.880	2.83	74.0	26.0	71.0	-0.269

TABLE 2 (continued)

Temp.	Time (min.)	Log Time	Area Ratio β_{101}/α_{200}	%α From Calibration	%β	X=Fraction Transformed x100	Log_1 Log [1 - X]
(125°C.)							
	100	2.000	3.13	73.7	26.3	71.8	-0.260
	217	2.336	3.55	71.4	28.6	78.2	-0.180
	1000	3.000	4.07	67.8	32.2	88.0	-0.036
150°C.	Quenched	-	0	100	0	0	-
	2	0.301	0.68	89.5	10.5	29.0	-0.827
	5	0.699	1.52	82.8	17.2	47.5	-0.553
	10	1.000	1.73	81.2	18.8	51.9	-0.498
	15	1.176	2.27	77.7	22.3	61.6	-0.382
	23	1.362	2.37	77.0	23.0	63.5	-0.358
	36	1.556	2.68	75.2	24.8	68.5	-0.300
	50	1.699	3.02	73.0	27.0	74.5	-0.227
	70	1.845	3.20	72.7	27.3	75.3	-0.217
	100	2.000	3.50	70.3	29.7	82.0	-0.128
	300	2.477	3.92	68.0	32.0	88.3	-0.031
	1007	3.003	3.87	68.2	31.8	88.0	-0.036

TABLE 3. DATA FOR DECOMPOSITION OF α IN ZINC-45% ALUMINUM

Temp.	Time (min.)	Log Time	Area Ratio β_{101}/α_{200}	% α From Calibration Curve	% β	X=Fraction Transformed x100
75°C.	Quenched	-	-	100	0	0
	7	0.845	0.17	96.3	3.7	11.1
	15.1	1.179	0.41	93.3	6.7	20.1
	25	1.398	0.76	89.7	10.3	30.9
	47	1.672	1.33	85.0	15.0	45.0
	76	1.880	1.83	81.7	18.3	55.0
	127	2.104	2.28	78.8	21.2	63.7
	216.5	2.335	2.72	76.2	23.8	71.4
	424	2.628	3.15	73.5	26.5	79.5
	1000	3.000	3.35	72.7	27.3	82.0
	2000	3.301	3.75	70.9	29.1	87.5
100°C.	Quenched	-	-	100	0	0
	5	0.699	0.63	90.8	9.2	28.2
	10	1.000	1.05	87.0	13.0	39.9
	16	1.204	1.65	82.5	13.5	53.7
	20	1.301	1.79	81.7	18.3	56.2
	25	1.398	1.82	81.6	18.4	56.5
	30	1.477	1.86	81.3	18.7	57.3
	35	1.544	1.97	80.7	19.3	59.2
	45	1.653	2.00	80.5	19.5	59.8
	60	1.778	1.95	80.7	19.3	59.2
	100	2.000	2.73	76.0	24.0	73.6
	174	2.240	2.86	75.4	24.6	75.3
	300	2.477	3.47	72.0	28.0	85.8
	317	2.501	3.37	72.5	27.5	84.3
	1000	3.000	3.60	71.4	28.6	87.7
125°C.	Quenched	0	0	100	0	0
	2	0.301	0.74	89.4	10.6	32.9
	5	0.699	1.20	85.6	14.4	44.7
	10	1.000	1.60	82.5	17.5	54.3
	15	1.176	1.76	81.4	18.6	57.7
	35	1.544	2.10	79.2	20.8	64.6
	63	1.799	2.30	78.0	22.0	68.3
	72	1.857	2.62	76.0	24.0	74.5
	83	1.919	2.87	74.7	25.3	78.5
	240	2.380	3.30	71.4	28.6	88.7
	1000	3.000	3.51	71.0	29.0	90.0

TABLE 3 (continued)

Temp.	Time (min.)	Log Time	Area Ratio β_{101}/α_{200}	% α From Calibration Curve	% β	X=Fraction Transformed x100
150°C.	Quenched		0.035	100	0	
	1	0	.84	88.0	12	37.7
	3	.477	1.20	85.0	15	47.2
	6	.778	1.37	83.7	16.3	51.2
	11	1.041	2.05	79	21	66
	15	1.176	2.45	78.3	21.7	68.2
	20	1.301	2.45	76.5	23.5	73.8
	23	1.362	2.30	77.4	22.6	71.0
	31.5	1.498	2.70	75.0	25.0	78.6
	54	1.732	2.86	74.0	26.0	81.7
	61.5	1.789	2.78	74.5	25.5	80.2
	100	2.000	3.10	72.6	27.4	86.2
	300	2.477	3.41	70.8	29.2	91.8
	967	2.985	3.56	69.3	30.7	96.5
	6630	3.821	3.75	68.2	31.8	100

TABLE 4. DATA FOR DECOMPOSITION OF α IN ZINC-55% ALUMINUM

Temp.	Time (min.)	Log Time	Area Ratio β_{101}/α_{200}	% α From Calibration Curve	% β	X=Fraction Transformed x100
75°C.	0	-	0	100	0	0
	20	1.301	.07	98.2	1.8	7.32
	22	1.342	0.12	97.3	2.7	11.0
	30	1.477	0.21	95.7	4.3	17.5
	50	1.699	0.29	94.2	1.8	7.32
	60	1.778	0.45	92.5	7.5	30.5
	80	1.902	0.95	88.0	12	48.8
	100	2.000	1.02	87.2	12.7	51.8
	145	2.161	1.22	86.0	14.0	56.8
	190	2.278	1.30	85.0	15.0	60.9
	440	2.643	1.72	82.6	17.4	70.7
	1000	3.000	1.78	81.8	18.2	74.1
	2000	3.301	2.11	79.7	20.3	82.5
	5000	3.699	2.42	77.9	22.1	90
100°C.	Quenched	-	0	100	0	0
	5	.699	.16	96.4	3.6	15.1
	10	1.000	.25	95.0	5.0	21.0
	15	1.176	.90	88.3	11.7	49.8
	20	1.301	.60	90.0	10.0	42.0
	25	1.398	1.10	86.2	13.8	58.0
	35	1.544	1.13	86.5	13.5	56.7
	50	1.699	1.32	85.0	15.0	63.0
	100	2.000	1.34	84.7	15.3	64.2
	250	2.398	1.62	82.8	17.2	72.2
	450	2.653	1.77	81.8	18.2	76.4
	750	2.875	1.91	81.2	18.8	78.9
	2000	3.301	2.44	77.8	22.2	96.2
	3000	3.477	2.79	75.7	24.3	99.6
	30*	1.477	1.03	87.1	12.9	54.2
	100*	2.000	1.35	84.5	15.5	65.0
	250*	2.398	1.59	82.5	17.5	73.5
125°C.	Quenched	-	0	100	0	0
	2	0.301	0.09	97.6	2.4	10.2
	2.5	0.398	0.12	97.2	2.8	11.9
	5	0.699	0.58	90.8	9.2	39.3
	10	1.000	0.90	88.1	11.9	50.8
	20	1.301	1.25	85.0	15.0	64.1
	35	1.544	1.41	84.0	16.0	68.3

TABLE 4 (continued)

Temp.	Time (min.)	Log Time	Area Ratio β_{101}/α_{200}	% α From Calibration Curve	% β	X=Fraction Transformed x100
(125°C.)	66	1.819	1.56	82.8	17.2	73.5
	100	2.000	1.69	81.9	18.1	77.3
	300	2.477	1.94	80.3	19.7	84.2
	1000	3.000	2.37	77.8	22.2	94.9
150°C.	Quenched	-	0	100	0	0
	4.5	0.653	1.21	85.0	15.0	65.0
	8	0.903	1.18	85.2	14.8	64.3
	10	1.000	1.20	84.9	15.1	65.2
	15	1.176	1.34	83.9	16.1	70.0
	25	1.398	1.50	82.8	17.2	74.7
	50	1.699	1.68	81.3	18.7	81.2
	100	2.000	1.88	79.9	20.1	87.2
	200	2.301	2.08	78.8	21.2	92.1
	500	2.699	2.27	77.6	22.4	97.5

* Delayed quench tests

TABLE 5. ACTIVATION ENERGIES ($\frac{\text{kcal.}}{\text{mole}}$) FOR THE ISOTHERMAL DECOMPOSITION OF METASTABLE α-PHASE IN ZINC-ALUMINUM ALLOYS

Amount of α Transformed	Zinc-40% Aluminum	Zinc-45% Aluminum	Zinc-55% Aluminum
30	19.2	20.5	23.3
40	19.5	20.7	23.3
50	18.6	20.7	22.7
60	24.6	21.3	25.0

TABLE 6. ROOM TEMPERATURE DECOMPOSITION OF α

Alloy % Al	Time (min.)	Area Ratio $\beta_{101} / \alpha_{200}$	% α	% β	Fraction Transformed x100
40	330	0.37	93.7	6.3	10.1
	480	0.70	89.3	10.7	17.1
	1020	0.99	87.5	12.5	20.0
	1830	3.36	74.2	25.8	41.3
	2520	2.31	86.2	13.8	22.1
	23110	2.15	85.0	15.0	24.0
	31900	3.09	72.5	27.5	44.0
	45330	4.07	69.2	30.8	49.3
	62100	4.02	69.5	30.5	48.8
45	120	.10	98.0	2.0	3.0
	340	0.53	91.8	8.2	12.3
	495	0.93	87.9	12.1	18.1
	1050	1.54	83.3	16.7	25.1
	2530	2.36	78.3	21.7	32.6
	23100	3.72	71.1	28.9	43.3
	31900	3.74	70.9	29.1	43.7
	45340	4.03	69.2	30.8	46.2
	62100	4.34	67.8	32.2	48.2
55	480	0.07	88.3	11.7	15.5
	730	0.15	86.4	13.6	18.0
	2460	0.33	84.2	15.8	20.9
	6360	0.75	79.8	20.2	26.8
	8760	1.23	75.5	24.5	32.5
	31400	2.30	68.8	31.2	41.3
	40150	2.04	70.3	29.7	39.4
	57800	2.07	70	30	39.8
	71800	2.24	68.9	31.1	41.2